

# Hyper-temporal remote sensing for digital soil mapping: Characterizing soil-vegetation response to climatic variability<sup>☆</sup>



Jonathan J. Maynard<sup>\*</sup>, Matthew R. Levi

USDA-ARS, Jornada Experimental Range, P.O. Box 30003, MSC 3JER, New Mexico State University, Las Cruces, NM 88003, United States

## ARTICLE INFO

### Article history:

Received 30 April 2016

Received in revised form 22 August 2016

Accepted 21 September 2016

Available online xxxx

### Keywords:

Remote sensing  
Digital soil mapping  
Climatic variability  
Hyper-temporal  
Machine learning  
Landsat

## ABSTRACT

Indices derived from remotely-sensed imagery are commonly used to predict soil properties with digital soil mapping (DSM) techniques. The use of images from single dates or a small number of dates is most common for DSM; however, selection of the appropriate images is complicated by temporal variability in land surface spectral properties. We argue that hyper-temporal remote sensing (RS) (i.e., hundreds of images) can provide novel insights into soil spatial variability by quantifying the temporal response of land surface spectral properties. This temporal response provides a spectral 'fingerprint' of the soil-vegetation relationship which is directly related to a range of soil properties. To evaluate the hyper-temporal RS approach, this study first reviewed and synthesized, within the context of temporal variability, previous research that has used RS imagery for DSM. Results from this analysis support the notion that temporal variability in RS spectra, as driven by soil and climate feedbacks, is an important predictor of soil variability. To explicitly evaluate this idea and to demonstrate the utility of the hyper-temporal approach, we present a case study in a semiarid landscape of southeastern Arizona, USA. In this case study surface soil texture and coarse fragment classes were predicted using a 28 year time series of Landsat TM derived normalized difference vegetation index (NDVI) and modeled using support vector machine (SVM) classification, and results evaluated relative to more traditional RS approaches (e.g., mono-, bi-, and multi-temporal). Results from the case study show that SVM classification using hyper-temporal RS imagery was more effective in modeling both soil texture and coarse fragment classes relative to mono-, bi-, or multi-temporal RS, with classification accuracies of 67% and 62%, respectively. Short-term transitions between wet and dry periods (i.e., <6 months) were the dominant drivers of vegetation spectral variability and corresponded to the general timing of significant RS scenes within in our SVM models, confirming the importance of spectral variability in predicting soil texture and coarse fragment classes. Results from the case study demonstrate the efficacy of the hyper-temporal RS approach in predicting soil properties and highlights how hyper-temporal RS can improve current methods of soil mapping efforts through its ability to characterize subtle changes in RS spectra relating to variation in soil properties.

Published by Elsevier B.V.

## 1. Introduction

Spectral indices derived from satellite imagery are important predictors used for digital soil mapping (DSM) (e.g., Boettinger et al., 2008; Grunwald, 2009; McBratney et al., 2003; Peng et al., 2015; Scull et al., 2003). DSM studies typically incorporate spectral indices from one or two image dates (or composites) into soil prediction models (i.e.,

mono- and bi-temporal), with far fewer instances of DSM models that incorporate multiple image dates (i.e., multi-temporal analysis). These trends are largely the result of: (i) historical barriers (e.g., financial, computational, analytical) that have prevented the use of high frequency imagery, and (ii) an underappreciation of the unique information encapsulated within the temporal response of land surface spectral properties. Recent technological and methodological advancements in the field of remote sensing (RS) are providing new opportunities for utilizing spectral indices derived from high frequency imagery stacks (e.g., MODIS, Landsat) for the modeling of soil properties and classes. Contrary to prior soil models that encapsulate a 'static' spectral view of the landscape (i.e., mono-temporal analysis), the use of hyper-temporal RS (i.e., hundreds of images) can uncover the temporal response of biophysical properties at the Earth's surface (e.g., vegetation), which in turn are linked in predictable ways to soil properties. In this paper we argue that hyper-temporal RS can provide novel insights into soil spatial

*Abbreviations:*  $\kappa$ , kappa statistic; PCC, percent correctly classified; PFT, plant functional type; RS, remote sensing; SVM, support vector machine.

<sup>☆</sup> Mention of a proprietary product does not constitute a guarantee or warranty of the products by the U.S. Government or the authors and does not imply its approval to the exclusion of other products that may be suitable.

<sup>\*</sup> Corresponding author at: USDA-ARS, Jornada Experimental Range, P.O. Box 30003, MSC 3JER, New Mexico State University, Las Cruces, NM 88003-8003, United States.

E-mail address: [jonathan.maynard@ars.usda.gov](mailto:jonathan.maynard@ars.usda.gov) (J.J. Maynard).

variability by quantifying the temporal response of each image pixel across a landscape.

Spectral indices provide information on soil properties and classes either directly through the imaging of bare soils (e.g., mineral indices, see Ben-Dor et al., 2008), or indirectly through the use of vegetation indices (e.g., NDVI) (Mulder et al., 2011). Given the predominance of vegetation across the Earth's land surface, a large portion of DSM efforts have incorporated vegetation indices into soil prediction models (Grunwald, 2009; Mulder et al., 2011). However, temporal variability in vegetation spectra resulting from seasonal changes in phenology and/or inter-annual soil-vegetation feedbacks to climate (e.g., El Niño-Southern Oscillation) can produce spurious results depending on the image date(s) chosen to derive vegetation indices. Consequently, previous studies using RS vegetation indices for DSM have employed two different methodologies to account for temporal variability. The first and most common methodology is to control for temporal variability by acquiring imagery that characterizes 'normal' conditions represented by an annual mean or multi-year mean composite image (Hengl et al., 2003; Page et al., 2013), or alternatively by a single image acquired during a specific time of year (e.g., annual peak biomass, dry season) (Chagas et al., 2013; Taghizadeh-Mehrjardi et al., 2015). The second and less common methodology is to characterize the temporal variability in vegetation spectra by utilizing bi-temporal (two images) or multi-temporal (three or more images) imagery, which can characterize differences in plant phenology, as well as changes driven by the soil-vegetation response to changes in climate.

While soil properties are largely static relative to vegetation, soils modulate the response of vegetation to climatic variability and in particular climatic extremes (i.e., physiological response to prolonged drought or elevated rainfall). Consequently, through quantifying temporal variability in land surface spectral properties (e.g., NDVI) we can gain greater insight into the spatial distribution of soil properties that regulate vegetation response (e.g., soil texture, water holding capacity, soil nutrient status). Changes in vegetative status occur on intra-annual time scales, reflecting increasing or decreasing plant vigor in response to available moisture. Alternatively, changes in fractional vegetation cover reflect an inter-annual response to prolonged periods of drought or abnormal wetness. From a remote sensing perspective, a single RS image provides a 'snapshot' of surface properties (e.g., variability in surface greenness relating to the distribution of plant functional types); however, areas identified as having similar spectral properties in a given image may experience vastly different temporal responses to variation in precipitation or temperature. Consequently, the accurate prediction of soil properties based on the soil-vegetation relationship and its response to climatic variability requires a measurement frequency that can adequately characterize these temporal dynamics. Thus, in contrast to bi-temporal and multi-temporal RS approaches which characterize seasonal and/or inter-annual variability at coarse temporal resolutions, hyper-temporal RS can characterize both intra- and inter-annual variability at a high temporal resolution, allowing the detection of subtle changes in RS spectra relating to soil variability. The temporal response of vegetation spectra derived from hyper-temporal RS provides a spectral 'fingerprint' of the soil-vegetation-climate relationship which is directly related to a range of soil properties. It should be recognized, however, that in highly managed ecosystems where the spectral signature of the landscape is artificially manipulated (e.g., agriculture), this approach will not likely produce reliable results unless those spectral changes can be accounted for (e.g., compiling all scenes across a time series when the area of interest is in corn production).

This study had two main objectives. The first objective was to review and synthesize, through the lens of temporal variability, previous research examining the use of RS imagery for DSM. The second main objective of this study was to test the utility of using hyper-temporal Landsat NDVI for predicting surface soil texture and coarse fragment classes in a semiarid landscape of southeastern Arizona, USA; and to evaluate these results relative to more traditional RS approaches (e.g., mono-, bi-, or multi-temporal).

## 2. Review and synthesis of RS applications for DSM: accounting for temporal variability

A wide range of RS data is now available for most regions of the world which presents many opportunities for predicting soil properties; hence, several reviews have been devoted to the use of RS in soil mapping (Grunwald et al., 2015; Mohanty, 2013; Mulder et al., 2011). A central premise in the estimation of soil properties using RS data is the existence of a predictable relationship between the spectral response measured by the sensor and the magnitude of the property of interest (Mulder et al., 2004). Several factors affect this relationship including the optical properties of the land surface (e.g., soil color, soil roughness, vegetation structure, leaf spectral properties); the effects caused by the spatial and temporal resolution of the sensor relative to the spatial structuring and temporal dynamics of the landscape; and finally environmental factors such as topography, sun elevation, and haze (Kerr and Ostrovsky, 2003). Consequently, the coupling of remote sensing and soil measurements has often produced mixed results due to the effects of the above stated factors, and in particular the inadequate accounting of temporal variability in RS spectra.

A summary of recent studies that have applied RS vegetation indices for soil property prediction is presented in Table S1. Our review of the literature was focused on how DSM studies account for and utilize temporal variability in RS spectra with a specific focus on the use of vegetation indices as covariates. DSM studies that utilize RS account for temporal variability in different ways and can be generally organized into four categories according to the number of images used: mono-temporal, bi-temporal, multi-temporal, and hyper-temporal.

Mono-temporal analysis, or the use of a single image, is the most common type of RS used for DSM. Mono-temporal analysis is most suited for properties that are temporally static, such as geology, parent material and other soil properties that can be identified by characterizing land surface color. For example, features like iron oxide, carbonate radicals, clay hydroxides, calcareous sediment, gypsiferous and natric soils are effectively identified with indices from multi-spectral RS (Bachofer et al., 2015; Boettinger et al., 2008; Nield et al., 2007). These types of applications require either adequate detection of the soil background (e.g., areas with minimal vegetation, periods of plant senescence) or the imaging of bare soils which requires the removal of all non-soil pixels (e.g., vegetation, water) prior to model development (Bachofer et al., 2015; Dutta et al., 2015; Nawar et al., 2015; Shabou et al., 2015). However, in many regions of the world the imaging of bare soils is not feasible due to extensive vegetation cover. As a result, many soil prediction models have applied vegetation indices (often in concert with other indices) derived from single image dates to predict a wide range of properties such as soil organic matter, salinity, phosphorus, physical soil properties and soil classes (Table S1). Since vegetation indices are temporally dynamic, the timing of imagery acquisition can strongly influence model development. To account for this, many studies have adopted the technique of aggregating multiple image dates to a single value (e.g., mean, maximum), which produces a representative, high quality image for a study area (Hengl et al., 2003; Kunkel et al., 2011; Page et al., 2013; Walker et al., 2003). For example, Page et al. (2013) produced an integrated NDVI representing the sum of both five and 10 year NDVI time series data to map soil carbon. Even though this approach utilizes multiple image dates, it does not exploit the temporal variability of image spectra within the model. While mono-temporal RS has been shown to be effective in predicting many soil properties, incorporating additional spectral variability (i.e., bi-temporal or multi-temporal RS) can improve model predictions for some soil properties (Blasch et al., 2015).

Bi-temporal RS, or the use of two images within a year or between years, is used to capture high magnitude changes in RS spectra/indices that may enhance soil prediction models (e.g., seasonal variation, soil moisture status). A common approach is to acquire imagery during both 'wet' and 'dry' conditions to capture phenological variation of

vegetation (Heung et al., 2016; Rivero et al., 2007). For example, Brungard et al. (2015) created indices (including NDVI) from Landsat scenes representing both peak and non-peak vegetation growth to predict soil taxonomic groups and found that for a semi-arid region of New Mexico, indices from the 'wet' scene were more important than those from the 'dry' scene. The bi-temporal approach has been used to map soil properties such as salt-affected soils, phosphorus, taxonomic groups, and soil landscape classes, which illustrates the utility of strategically incorporating multiple image dates into soil prediction models (Table S1).

Multi-temporal RS is characterized as having more than two image dates. This approach captures intra- and/or inter-annual variability at coarse temporal resolutions, and generally includes either a seasonal time series or a multi-year time series where images are collected during the same time of year (e.g. peak biomass). Time series of NDVI are effective in identifying differences in soil properties and land degradation across a range of landscapes (Lozano-Garcia et al., 1991; Omuto and Shrestha, 2007; Schmidt and Karnieli, 2000). Multi-year image analysis from the same time of year is used to characterize inter-annual variability and has been effective in modeling soil properties. For example, Omuto and Shrestha (2007) used 11 Landsat scenes from the driest month of the year to predict soil degradation classes and hydraulic soil properties in eastern Kenya. Basnyat et al. (2005) used repeated Landsat NDVI from the same time following seeding to develop soil management zones in southwestern Saskatchewan. Relative to mono- or bi-temporal image analysis, multi-temporal image analysis has been more commonly used to predict dynamic soil properties like organic matter, soil moisture, water table depth and gas flux (Table S1). Multi-temporal RS is also useful for predicting static properties such as taxonomic groups (Dobos et al., 2001; Lozano-Garcia et al., 1991) and soil texture (Shabou et al., 2015) due to the influence these properties have on the temporal dynamics of vegetation spectra.

The majority of studies presented in Table S1 represent mono-temporal RS (30 studies); with seven bi-temporal, and 19 multi-temporal studies. While our analysis identified 30 DSM studies from recent years (~20 years) that used mono-temporal RS, given the widespread and long-term use of RS over the past four decades there are likely additional examples not included in our review. Despite these potential omissions, it is clear that, (i) mono-temporal RS has been an important covariate in many DSM models, (ii) the use of multi-temporal RS in DSM studies is increasing, and (iii) incorporating increasing RS spectral variability into DSM warrants additional research to explicitly examine its potential for improving soil prediction models.

### 3. Modeling soil properties using hyper-temporal remote sensing: a case study in a semi-arid ecosystem

Hyper-temporal RS is capable of characterizing both intra- and inter-annual variability at a high temporal resolution, thus allowing the detection of subtle changes in RS spectra relating to variation in soil properties. Prior constraints (e.g., imagery cost, computational efficiency) on using hyper-temporal RS in DSM studies no longer exist due to continued advancements in the field of remote sensing. These advancements include: (i) free and open distribution of imagery (e.g., Landsat, see Woodcock et al., 2008), allowing the creation of dense pixel-based time series; (ii) significant advancements in image pre-processing (e.g., Landsat Ecosystem disturbance Adaptive Processing System (LEDAPS) algorithm) creating comparable imagery across time; (iii) increases in computation capacity, in particular cloud-based computing platforms such as Google Earth Engine (e.g., global-scale processing of Landsat, see Hansen et al., 2013); and (iv) advances in time series algorithms using high temporal resolution satellite image stacks (Kennedy et al., 2014; Main-Knorn et al., 2013; Verbesselt et al., 2010). Furthermore, advances in statistical data mining techniques (e.g., artificial neural networks, decision trees and support vector machines) have become powerful tools for predicting soil properties

using large multivariate datasets (Brungard et al., 2015; Heung et al., 2016; Taghizadeh-Mehrjardi et al., 2015). With these advancements it is now possible to use hyper-temporal RS image stacks to model the spatial distribution of soil properties and classes, and in particular those soil properties that regulate the temporal response of land surface biophysical properties (e.g., vegetation). Several recent examples have emerged, demonstrating the efficacy of hyper-temporal RS in predicting soil hydraulic properties such as water holding capacity (Araya et al., 2016), static soil properties such as taxonomic classes (Li et al., 2012), and dynamic soil properties like soil organic matter (Poggio et al., 2013).

In this study, we tested the efficacy of hyper-temporal RS for predicting soil texture and coarse fragment classes in an arid ecosystem in southeastern Arizona, USA. While previous studies have shown that aboveground productivity is highly correlated to precipitation in arid ecosystems (Jenerette et al., 2010; Williamson et al., 2012), recent work indicates that soil moisture largely controls aboveground greenness (Kurc and Benton, 2010; Schnur et al., 2010; Shepard et al., 2015; Wang et al., 2007). Soil texture exerts a dominant control on soil moisture conditions in arid ecosystems (i.e., <370 mm of precipitation), with coarse surface textures having the highest aboveground productivity due to rapid infiltration during rainfall events and reduced evaporative losses due to a low water-holding capacity (i.e., inverse texture hypothesis: Sala et al., 1988, 2015). Soil texture further influences soil moisture dynamics, with finer subsurface textures retaining moisture near the surface where it is available to shallow-rooted species (e.g., grasses) and coarser subsurface textures allowing deeper infiltration where it is only available to plants with extensive root systems (e.g., woody species) (McAuliffe, 1994; Shepard et al., 2015). Consequently, previous research has shown that grasses are more resilient to drought in soils with a high water holding capacity in the upper 1-m of the soil profile, while woody species tend to dominate on soils that promote deep infiltration (i.e., >1 m) (Gibbens et al., 2005; Yao et al., 2006).

As a result, variation in soil texture results in different temporal responses of soil moisture availability under changing climatic conditions, which in turn results in changes in vegetation characteristics, like vegetative condition (i.e., greenness) and fractional cover (changing phenology), that can be captured by optical remote sensing through detecting changes in spectral bands (e.g., near-infrared and visible reflectance bands) and/or indices (e.g., NDVI). For example, subsurface soil moisture (e.g. >30 cm) has been linked to measures of greenness at local spatial scales using soil moisture sensors and pheno-cams, providing evidence for edaphic controls on the spectral response of vegetation (Kurc and Benton, 2010). Additionally, previous studies have found links between NDVI and surface moisture (Farrar et al., 1994) and NDVI and root zone soil moisture (Adegoke and Carleton, 2002) at broad spatial scales. Accurate prediction or adequate differentiation between contrasting classes requires a measurement frequency that can detect subtle variation in temporal responses. Thus, a main objective of this study was to test the utility of using hyper-temporal Landsat NDVI for predicting surface soil texture and coarse fragment classes. Specific objectives were to: (i) examine RS spectral variability through time and its relationship to soil texture and coarse fragment classes, (ii) examine the relationship between precipitation and NDVI spectral variability, and (iii) evaluate the use of SVM classification for predicting soil texture and coarse fragment classes using hyper-temporal Landsat NDVI, as compared to more traditional RS approaches. We predict hyper-temporal spectral 'fingerprints' of different portions of the landscape will prove useful for modeling the spatial variability of soil properties.

## 4. Methods

### 4.1. Study area

The study area is a 6065 ha landscape in southeastern Arizona located 30 km north of the city of Wilcox in Cochise County (Fig. 1). Elevation

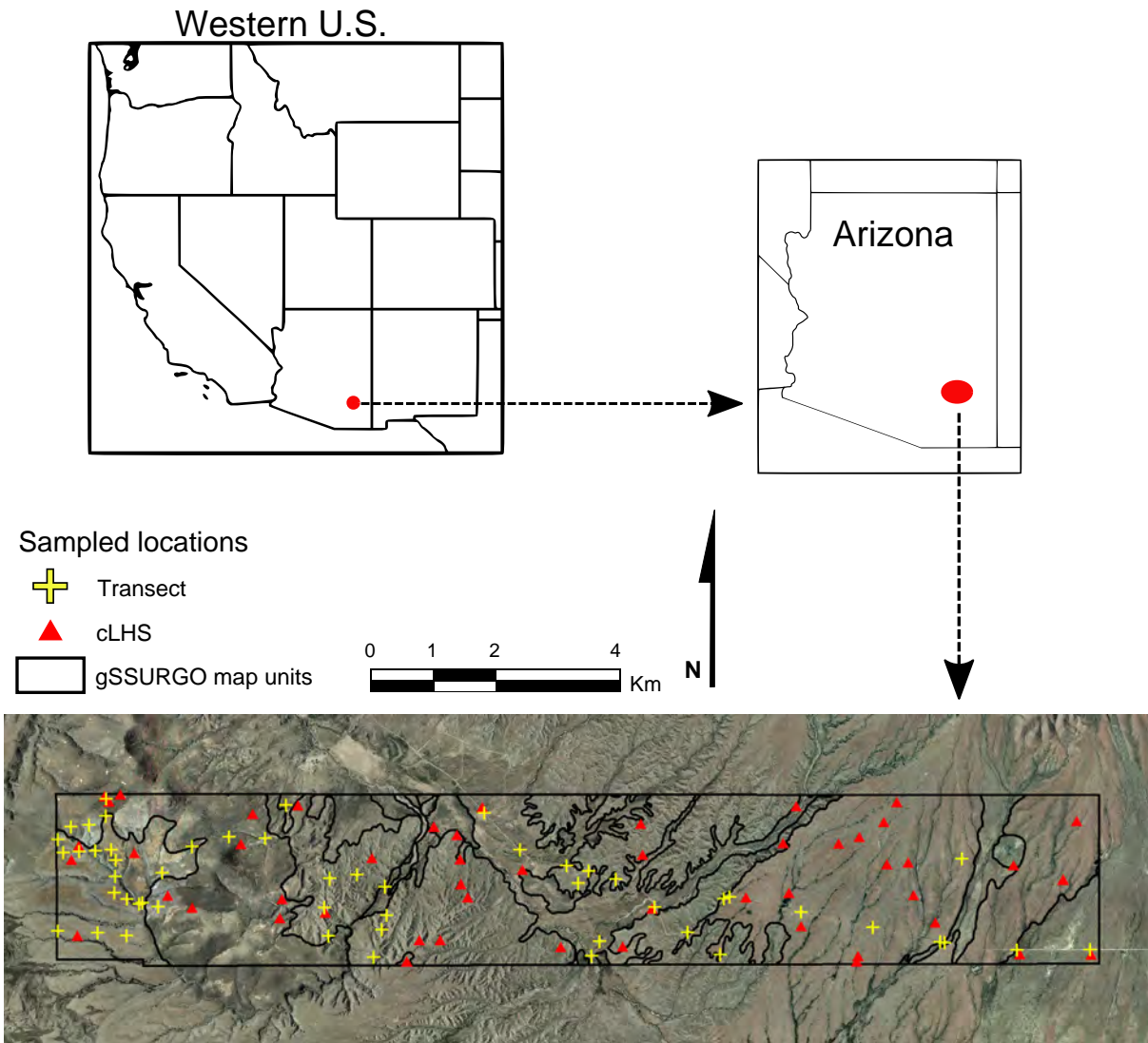


Fig. 1. Location of the study area (6265 ha) in a semiarid rangeland landscape of southeastern Arizona. The distribution of sampled locations from initial soil survey transects and a conditioned Latin Hypercube design (cLHS) (Levi and Rasmussen, 2014) represented the distribution of soil survey map units (black lines).

ranges from 1273 to 1655 m above sea level within the study area and adjacent mountain ranges to the east and west have maximum elevations of 3267 and 2336 m, respectively. Parent materials are primarily sedimentary basin fill deposits in the form of alluvial fans ranging in age from Holocene to early Miocene-aged (~20 Ma) materials (Reynolds et al., 2000; Wilson and Moore, 1958). A large portion of the study area is comprised of relatively easily discernable parent materials where granitic alluvium dominates the eastern portion and volcanic alluvium and basalt hills make up the western portion. The center of the study area is a mixture of lacustrine deposits that contain abundant soluble salts including carbonates and gypsum (Melton, 1965). A recent soil survey mapped Argiustolls, Paleargids, Haplocambids, Haplogypsis, Gypsiteorrerts, Torrifluvents, Torriorrhents, riverwash and rock outcrop within the study area (Soil Survey Staff, 2011). A more detailed description of the study area can be found in Levi and Rasmussen (2014).

The study area has a semiarid climate and receives a bi-modal distribution of rainfall during the summer and winter with mean annual precipitation ranging from 403 to 472 mm (PRISM Climate Group, 2008). Spatial and temporal patterns of precipitation are largely controlled by the North American Monsoon system (Sheppard et al., 2002) resulting in unique responses of vegetation (Sponseller et al., 2012). Mean annual air temperature is approximately 16.5 °C with a range from 9 to 25 °C.

The soil moisture regimes are aridic and ustic and the soil temperature regime is thermic (15–22 °C) (Soil Survey Staff, 2011).

Vegetation in the study area is characteristic of semi-desert grassland and includes a variety of grasses, forbs, shrubs, leaf succulents, and cacti common to the Chihuahuan and Sonoran Deserts (Brown and Lowe, 1978; Brown, 1982). Upland landscape positions are generally dominated by perennial grasses (*Bouteloua* spp., *Eragrostis* spp.) with scattered shrubs (*Prosopis* spp., *Larrea tridentata*) whereas drainages have greater shrub cover. In some portions of the lowland landscapes subject to flooding, monotypic stands of *Sporobolus wrightii* are present, which is a large, warm-season, perennial bunchgrass common to southeastern Arizona that can grow nearly 2 m in height (Casady et al., 2013).

#### 4.2. Sample design, field sampling and laboratory analyses

Soil samples were available from two different sources. Field transects for initial soil survey efforts of the southwestern part of Graham County Arizona, USA (Soil Survey Staff, 2011) were collected in 2010. We used soil profile descriptions for 54 point locations within our study area that included estimates of surface soil texture class from hand texturing of experienced NRCS soil scientists. An additional 52 points were sampled as part of a related research study (Levi and Rasmussen, 2014). Field locations for the research study were

determined with a conditioned Latin Hypercube (cLHS) sample design (Minasny and McBratney, 2006) using environmental covariates selected with an iterative principle component data reduction (Levi and Rasmussen, 2014). A total of 52 soil profiles were sampled by genetic soil horizon from 0 to 30 cm in April and May of 2011. Air-dried soils were sieved through a 2 mm mesh and pretreated with sodium acetate (NaOAc - pH 5) to remove soluble salts and sodium hypochlorite (NaOCl - pH 9.5) to remove organic matter (Jackson, 2005). Following dispersion with sodium hexametaphosphate, soil particle size distribution was determined using a Beckman Coulter LS 13 320 Laser Diffraction Particle Size Analyzer. Surface soil texture class for the research samples were determined from laboratory sand, silt and clay fractions. Detailed descriptions of the sampling design and laboratory analyses from the research study are presented in Levi and Rasmussen (2014). We excluded a total of three sample points with underrepresented soil texture classes ( $n < 3$ ) to facilitate model development and a total of 103 sample points were used. We elected to model texture class because sand, silt, and clay estimates were not available for the soil survey field transects which account for half of our 103 final sample points.

#### 4.3. Standardized precipitation index

To evaluate the effects of precipitation patterns on the general availability of soil moisture for plants (i.e., wet or dry soil conditions), we used daily precipitation data from a nearby (~15 miles away) meteorological station that is part of the Arizona Meteorological Network (<http://ag.arizona.edu/azmet/index.html>; Bonita station) to calculate the standardized precipitation index (SPI) between the years 1987–2011. The SPI is a probability-based indicator that depicts the degree to which accumulative precipitation for a specific time period departs from the average state (Mckee et al., 1993). Since the SPI is standardized, an index of zero indicates the median precipitation amount (i.e., normal conditions), while drought conditions are indicated by negative values (i.e., -2 for exceptionally dry) and wet conditions are indicated by positive values (i.e., 2 for exceptionally wet). SPI can be calculated across a range of time scales, with short time scales (i.e., weeks), representing event-driven changes in water availability, relating to dynamic ecosystem properties (e.g., annual grass emergence); and longer time scales (i.e., years) relating to the cumulative effects of prolonged drought or wetness (e.g., vegetation dieback or shifts in plant functional types). In arid regions with highly seasonal distributions of precipitation, the SPI calculated at very short time scales (<1 month) has been shown to produce unreliable results for characterizing abnormal dryness or wetness due to the high occurrence of no-rain cases which results in a highly skewed distribution (Wu et al., 2007). Consequently, we selected time scales ranging from 1 to 36 months, to characterize both short- and long-term patterns.

#### 4.4. Landsat image acquisition and pre-processing

All available Landsat -Thematic Mapper (TM) imagery between 1984 and 2012 (16-day frequency) was acquired from USGS ESPA, totaling 530 scenes (Path 33/Row 37). The Landsat imagery was orthorectified and radiometrically calibrated to surface reflectance with the LEDAPS algorithm (Masek et al., 2006). Quality assessment (QA) masking was performed using the CFMASK algorithm (Zhu and Woodcock, 2014), masking all pixels identified as containing clouds, cloud shadow, water, or snow. Missing observations due to QA masking or missing scenes (i.e., Landsat 5 scenes processed through NLAPS), were infilled for each pixel-based time series using linear interpolation. The infilling procedure resulted in a complete 16-day time series from June 6, 1984 to October 14, 2011, totaling 627 scenes.

Normalized difference vegetation index (NDVI) is the most commonly used band ratio in ecological research and has been widely used in rangeland studies, although with varying levels of success (Anderson et al., 1993; Kawamura et al., 2005; Purevdorj et al., 1998;

Sankey and Weber, 2009; Wylie et al., 2002; Zha et al., 2003). The limitations of using NDVI in arid ecosystems have been well documented, including the effects of exposed soil, standing dead vegetation and litter on the spectral response (Gao et al., 2000; Huete, 1988; Richardson and Wiegand, 1977). Despite these limitations, preliminary analysis using NDVI and MSAVI (Modified Soil Adjusted Vegetation Index) showed that NDVI produced more accurate results in model prediction. The Landsat TM surface reflectance product contains a precomputed NDVI layer that was used in this study. NDVI is calculated from the red and NIR band values using the standard formula of:

$$NDVI = (\rho_{NIR} - \rho_{Red}) / (\rho_{NIR} + \rho_{Red}) \quad (1)$$

A seasonal-trend time series decomposition procedure based on local polynomial regression fitting (LOESS) smoothing was performed on each pixel stack ( $n = 70,634$ ), decomposing the time series into trend, seasonal, and remainder components (Cleveland et al., 1990). The trend and seasonal components were recombined, resulting in a filtered seasonal-trend time series for each pixel stack. The remainder component contains signal noise that was not removed during the prior preprocessing steps, in addition to a fraction of the true signal that the seasonal and trend models were unable to fit. This small loss of information associated with model fitting was considered acceptable given the increase in signal-to-noise ratio resulting from the filtering procedure. Fig. 2 illustrates the connection between Landsat time series decomposition and the soil prediction model. All image processing was done using R statistical software (R Core Team, 2015). Time series decomposition was done using the 'stl' function in the 'stats' package. The linear interpolation infilling procedure was done using the 'zoo' package (Zeileis and Grothendieck, 2005).

#### 4.5. Soil prediction model

Support vector machine (SVM) classification models were developed using the caret package (Kuhn, 2008) in R (R Core Team, 2015) to predict soil texture class and coarse fragment class across the study area. SVM is a supervised classification technique based on statistical learning theory that has gained popularity in the environmental sciences due to its effectiveness as a non-linear classifier in high dimensional spaces (Yang et al., 2006). In the machine learning process, a dataset that is representative in the domain of interest is used to train the machine learning algorithm, where it 'learns' the connections between features of the training data and a specified target concept (e.g., soil texture class). Additionally, SVM models perform well when trained with sparse and noisy input data and are highly resistant to overfitting (Kuhn and Johnson, 2013). Thus SVM models are highly generalizable, which allows for appropriate predictions from out-of-sample data.

SVM model development was performed by first selecting an appropriate kernel and determining optimal hyper-parameters relating to the selected kernel based on a tuning procedure. In this study we used the radial-basis kernel which is one of the most commonly used SVM kernels in soil and environmental studies (Twarakavi et al., 2009). Optimal estimation of SVM hyper-parameters was performed using a grid-based search approach, where all possible combinations of hyper-parameters were modeled using the training dataset, with each model evaluated using 10-fold cross-validation. Hyper-parameters from the cross-validated model with the highest kappa statistic ( $\kappa$ ) where chosen and used in subsequent model building (see Section 4.6 for more details about  $\kappa$ ).

Four types of SVM models were created: mono-temporal, bi-temporal, multi-temporal, and hyper-temporal. Mono-temporal models consisted of a single image that approximated annual maximum NDVI (image date closest to 01 September) for a given year. Bi-temporal models consisted of two images that approximated annual maximum and minimum NDVI (image dates closest to 01 September and 01 February) for a given year. Multi-temporal models included the annual

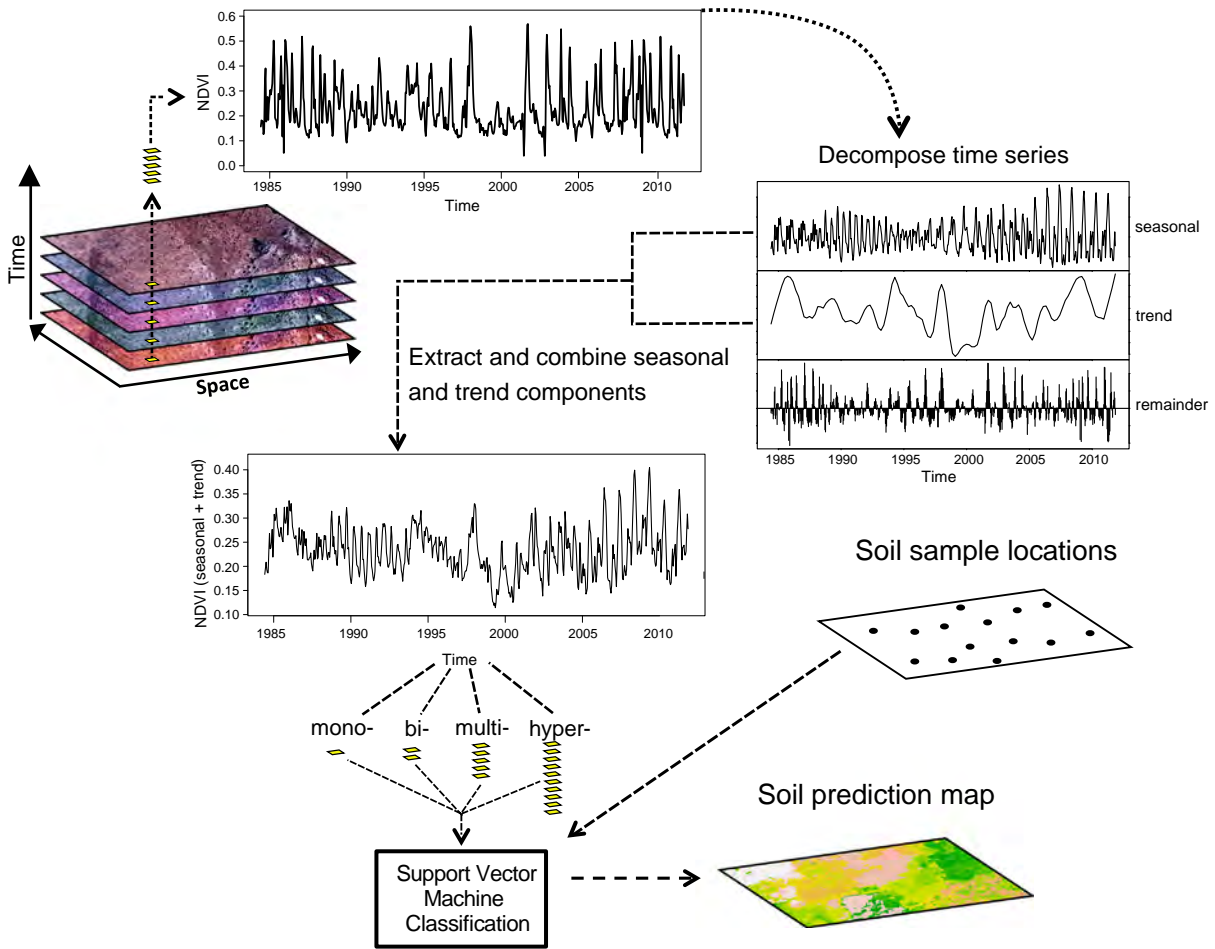


**Fig. 2.** Conceptual workflow showing the compilation of Landsat NDVI layers from 1984 to 2011, the decomposition and extraction of the seasonal and trend components of the time series for each pixel stack, and the integration of the modified time series and sampled field data into a support vector machine classification model to produce soil property prediction maps.

maximum NDVI from each year within the 28-year time-series and hyper-temporal models included every image within the 28-year time-series ( $n = 627$ ). Although SVM models are highly resistant to non-informative predictors (Kuhn and Johnson, 2013), two feature selection procedures were employed sequentially for the multi- and hyper-temporal models to identify and remove any redundant or non-informative covariates. First, a pairwise correlation analysis algorithm was used to identify and remove covariates with the highest degree of multi-collinearity. The algorithm first calculates a correlation matrix of all covariates; then sequentially evaluates all covariate pairs above a correlation threshold; and finally retains the covariate from each pair with the lowest average correlation with the remaining covariates. A correlation threshold of 0.9 was chosen for this study. Following the initial covariate filtering, genetic algorithm (GA) feature selection was performed on the reduced covariate dataset for both soil texture and coarse fragment classes. GA feature selection performs multiple iterations of covariate optimization, where each covariate is evaluated relative to the dependent variable, and external 10-fold cross-validation performed to prevent model overfitting (Kuhn and Johnson, 2013). Due to the highly unbalanced class size distribution for the soil coarse fragment classes, we applied class weights within our SVM coarse fragment models to prevent the extreme over prediction of the 0–15% class.

4.6. Model validation

The splitting of observation data into separate training and test sets is a standard approach used to evaluate model performance in many DSM studies (e.g., Henderson et al., 2005; Rad et al., 2014). However,

this approach only represents model performance for one pair of testing and training sets and can result in accuracy metrics with high variance when sample sizes are low or when sample class sizes are highly imbalanced (Kuhn and Johnson, 2013). Consequently, we employed repeated 10-fold cross-validation (R10FCV) with 10 repetitions on our entire dataset ( $n = 103$ ). R10FCV was used to select optimal tuning parameters and to evaluate model performance of our final model for texture class and coarse fragment class. Average accuracy metrics were calculated over the 10 repetitions of R10FCV. Model predictions and corresponding observation from each of the 10 repeats of the R10FCV ( $n = 103$  per repeat) were compiled and used to create a cross-validated error matrix consisting of 1030 classification values per cross-validated model.

Model performance was assessed using the following metrics: percent correctly classified (PCC),  $\kappa$ , producer’s accuracy, and user’s accuracy. PCC is the proportion of test observations that are correctly classified; however, when the sample class distribution is highly unbalanced the PCC value may be inflated. For example, when a class has a low rate of occurrence, high PCC could result from classifying all observations as the largest class (Congalton and Green, 2008). The  $\kappa$  accounts for this by measuring the classification accuracy after accounting for the probability of chance agreement (Congalton and Green, 2008) and is calculated as:

$$\kappa = \frac{O - E}{1 - E} \tag{2}$$

where  $O$  is the observed accuracy and  $E$  is the expected accuracy based on the marginal total of the confusion matrix.  $\kappa$  values below 0.4

represent poor agreement, values between 0.4 and 0.8 represent moderate agreement, and values  $> 0.8$  represent strong agreement. The models with the highest  $\kappa$  from the tuning and covariate selection steps were determined to be the most accurate. Model performance of each individual class within the soil texture (e.g., clay, sandy loam) and coarse fragment classes were assessed with producer's and user's accuracy. Producer's accuracy is a measure of the proportion of sample points correctly classified for a given class relative to the number of observed points of that class, reflecting model accuracy in terms of how well the landscape can be mapped. User's accuracy is a measure of the proportion of sample points correctly classified for a given class relative to the number of predicted points of that class, reflecting model accuracy in terms of how reliable the classification map is to the user. For the hyper-temporal model of soil texture classes, model misclassification in terms of the proportion of observations of a given class that were predicted as an adjacent class (producer's accuracy), is presented using textural triangles. Results are presented using all 10 repeats of the R10FCV.

#### 4.7. gSSURGO

Gridded Soil Survey Geographic (gSSURGO) soil maps with a mapping scale ranging from 1:20,000 to 1:63,360 were created based on the dominant condition of soil texture and coarse fragment classes published in gSSURGO (Soil Survey Staff, 2015). Dominant condition of soil texture class and coarse fragment class was determined by aggregating the classes of each named soil component in a given map unit and representing the map unit with the dominant condition of the respective classes. gSSURGO was used as an external reference for visually comparing and assessing the spatial arrangement of modeled classes within the four different SVM models types (i.e., mono-, bi-, multi-, and hyper-temporal).

## 5. Results

### 5.1. Soil physical properties

Sampled soils represented a wide range of textures from sandy loam to clay (Fig. 3). The dominant soil texture class in the sampled surface soils was sandy loam followed by clay and clay loam. Both silt loam ( $n = 5$ ) and sandy clay loam textures ( $n = 6$ ) had the fewest number of samples. More than half of the samples had 0–15% coarse fragments. The number of samples in the 15–35% and  $> 35\%$  coarse fragment classes were similar.

### 5.2. NDVI temporal variability and covariate selection

Mean NDVI for all 103 sample locations shows considerable variability in seasonal amplitude across the time series (Fig. 4a). Variability in NDVI seasonal amplitude corresponds to precipitation patterns both at long and short time-scales. Several distinct climatic periods were identified during the study period (1984–2011) that represented dry, normal, and wet conditions (Fig. 4b). Delineating temporal patterns of precipitation anomalies is dependent upon the time-scale at which the SPI is calculated. We delineated climatic periods using coarse temporal scales (i.e., 30–35 months), thus accounting for the long-term effects of antecedent soil moisture on vegetation condition. Although the first three years of precipitation data (1984–1987) were missing from our 28-year time series, four general climatic periods were delineated, with a period of wet conditions (1987–1997), followed by dry conditions (1997–2005), followed by normal conditions (2005–2009), and then finally another period of dry conditions (2009–2011) (Fig. 4b). At short time-scales (i.e., 1–6 months) distinct and sporadic precipitation events result in highly dynamic fluctuations between abnormally wet and dry conditions, as shown by the high number of fluctuations in SPI along the time series at the shortest temporal scales (Fig. 4).

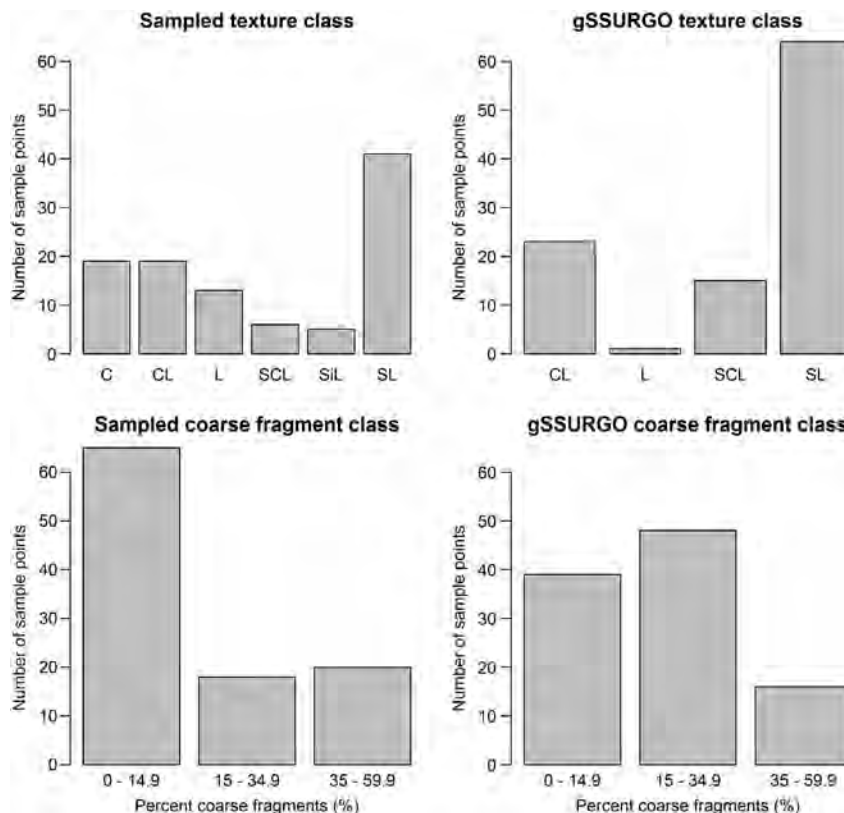
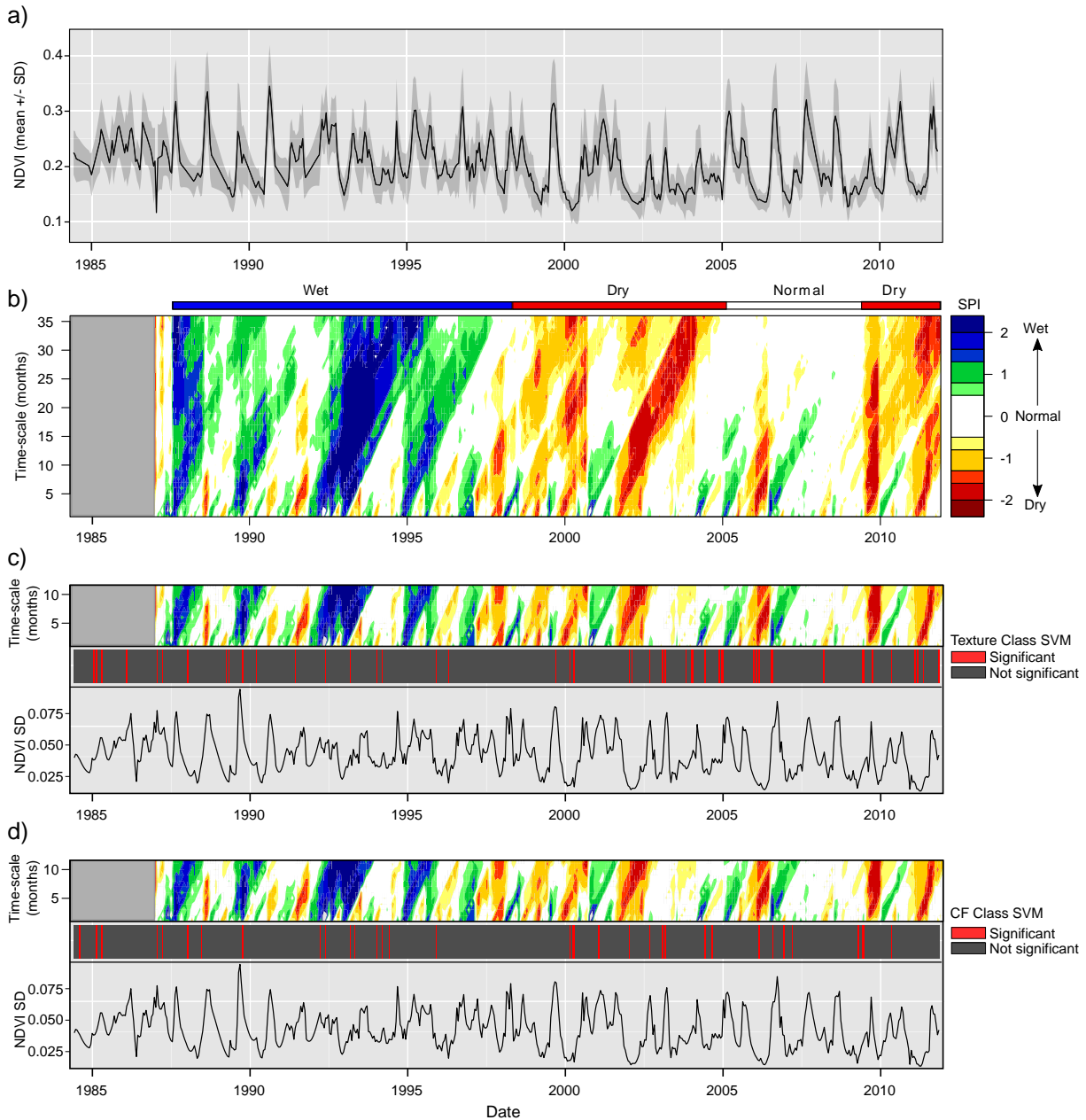


Fig. 3. Distribution of soil texture class and coarse fragment class for surface soil horizons at 103 sampled locations.



**Fig. 4.** Temporal patterns in (a) mean  $\pm$  1 standard deviation of NDVI calculated from Landsat pixels at all 103 sample locations; (b) standardized precipitation index (SPI) calculated across a range of time scales illustrating general climatic states (e.g., wet, dry, normal) at coarse temporal scales (~35 months) and event driven responses at short time-scales (~0–6 months); tri-panel illustrating relationship between significant SVM covariates (middle panel) and both short-term SPI (top panel) and NDVI standard deviation (bottom panel) for both (c) texture class and (d) coarse fragment class.

At broad temporal scales, the cumulative effect of precipitation patterns resulted in different generalized trends in NDVI within the identified climatic periods (Fig. 4a,b). For example, during the wet period from 1987 to 1997, long-term mean NDVI was relatively steady at  $\sim 0.21$ , followed by a drop during the dry period (1997–2005) to  $\sim 0.18$ , and then short-term increases during the normal period. However, at short time-scales the effects of variability in precipitation events resulted in inter-annual variability in the amplitude of NDVI during the different climatic periods (Fig. 4a). The standard deviation (SD) of NDVI at all 103 sample locations across the time series shows a seasonal pattern, with highest SD values occurring during periods of maximum NDVI (i.e., annual peak biomass), and lowest SD values occurring during periods of minimum NDVI (i.e., vegetative dormancy) (Fig. 4a).

Results from pairwise correlation analysis revealed that the multi-temporal dataset ( $n = 28$ ) had 17 NDVI images and the hyper-temporal

dataset ( $n = 627$ ) had 556 NDVI images with significant multicollinearity at the 0.9 threshold level. This resulted in initial reduced datasets with 11 and 71 NDVI images for the multi- and hyper-temporal datasets, respectively. Subsequent GA feature selection for soil texture class models revealed that 8 and 47 NDVI image dates were significant covariates for the multi-temporal and hyper-temporal datasets, respectively. For coarse fragment class models, GA feature selection revealed that 6 and 37 NDVI image dates were significant covariates for the multi-temporal and hyper-temporal datasets, respectively.

Significant covariates selected from the pairwise correlation and GA analysis for the hyper-temporal models were evaluated relative to NDVI temporal variability and climatic variability identified from the SPI analysis (Fig. 4c, d). Evaluating the temporal sequence of significant covariates for each hyper-temporal model within the context of short-term precipitation effects (1–6 month SPI) and NDVI variability (NDVI SD)

revealed a distinct pattern where significant scenes within each model occur after abrupt transitions between short-term climatic states (Fig. 4c, d).

### 5.3. SVM model performance

SVM models for soil texture and coarse fragment classes showed similar patterns of increasing model accuracy (i.e., PCC,  $\kappa$ ) with increasing temporal resolution. Significant variability in model performance for mono- and bi-temporal approaches was seen within each set of 28 models for soil texture and coarse fragment classes, both in terms of PCC and  $\kappa$  (Fig. 5). For both properties, hyper-temporal models had substantially higher PCC and  $\kappa$  values relative to mono-, bi-, and multi-temporal models (Fig. 5). Models for soil texture and coarse fragment classes performed similarly in terms of percent correctly classified (PCC), with accuracies ranging from 44 to 67% correct classification (Fig. 5a, c). The  $\kappa$  values for texture class models were in the 'poor agreement' category for mono-temporal ( $\kappa$  range: 0.00–0.25) and bi-temporal ( $\kappa$  range: 0.00–0.32) models, but in the 'moderate agreement' category for the multi-temporal ( $\kappa = 0.43$ ) and hyper-temporal ( $\kappa = 0.53$ ) models (Fig. 5b).  $\kappa$  values for coarse fragment models were all in the 'poor agreement' category, with very low  $\kappa$  values for mono- and bi-temporal models ( $\kappa$  range: 0.00–0.23), and only slightly higher  $\kappa$  values for multi-temporal ( $\kappa = 0.18$ ) and hyper-temporal ( $\kappa = 0.27$ ) models (Fig. 5d). The frequency distribution of texture classes was unbalanced, with the coarsest texture (sandy loam) having the highest number of observations, followed by the two finest texture

**Table 1**  
Error matrix for hyper-temporal model of soil texture classes.

| Class <sup>a</sup> | SVM error matrix |     |    |     |     |     |                 | UA (%) |
|--------------------|------------------|-----|----|-----|-----|-----|-----------------|--------|
|                    | Reference        |     |    |     |     |     |                 |        |
|                    | C                | CL  | L  | SCL | SL  | SiL |                 |        |
| Prediction C       | 131              | 40  | 20 | 0   | 0   | 0   | 69              |        |
| CL                 | 39               | 126 | 33 | 10  | 0   | 0   | 61              |        |
| L                  | 9                | 4   | 3  | 7   | 8   | 10  | 7               |        |
| SCL                | 0                | 0   | 0  | 0   | 0   | 0   | 0               |        |
| SL                 | 3                | 20  | 57 | 43  | 402 | 15  | 74              |        |
| SiL                | 8                | 0   | 17 | 0   | 0   | 25  | 50              |        |
| PA (%)             | 69               | 66  | 2  | 0   | 98  | 50  | PCC = 67%       |        |
|                    |                  |     |    |     |     |     | $\kappa = 0.53$ |        |

<sup>a</sup> C is clay, CL is clay loam, L is loam, SCL is sandy clay loam, SL is sandy loam, SiL is silt loam, UA is user's accuracy, PA is producer's accuracy, PCC is percent correctly classified,  $\kappa$  is kappa coefficient.

classes (clay and clay loam). Moderate texture classes (sandy clay loam and silt loam) were underrepresented (Fig. 3), however, good representation of the two textural extremes produced a moderately good  $\kappa$  for the hyper-temporal model. In contrast, the coarse fragment class distribution was highly unbalanced, likely contributing to the low  $\kappa$  values for all models (Fig. 5d, Table 2).

The most accurate mono- and bi-temporal models were selected to facilitate further comparisons between the four model types. Error matrices for the most accurate mono- and bi-temporal models, and the multi- and hyper-temporal models are presented in Tables 1, 2 and

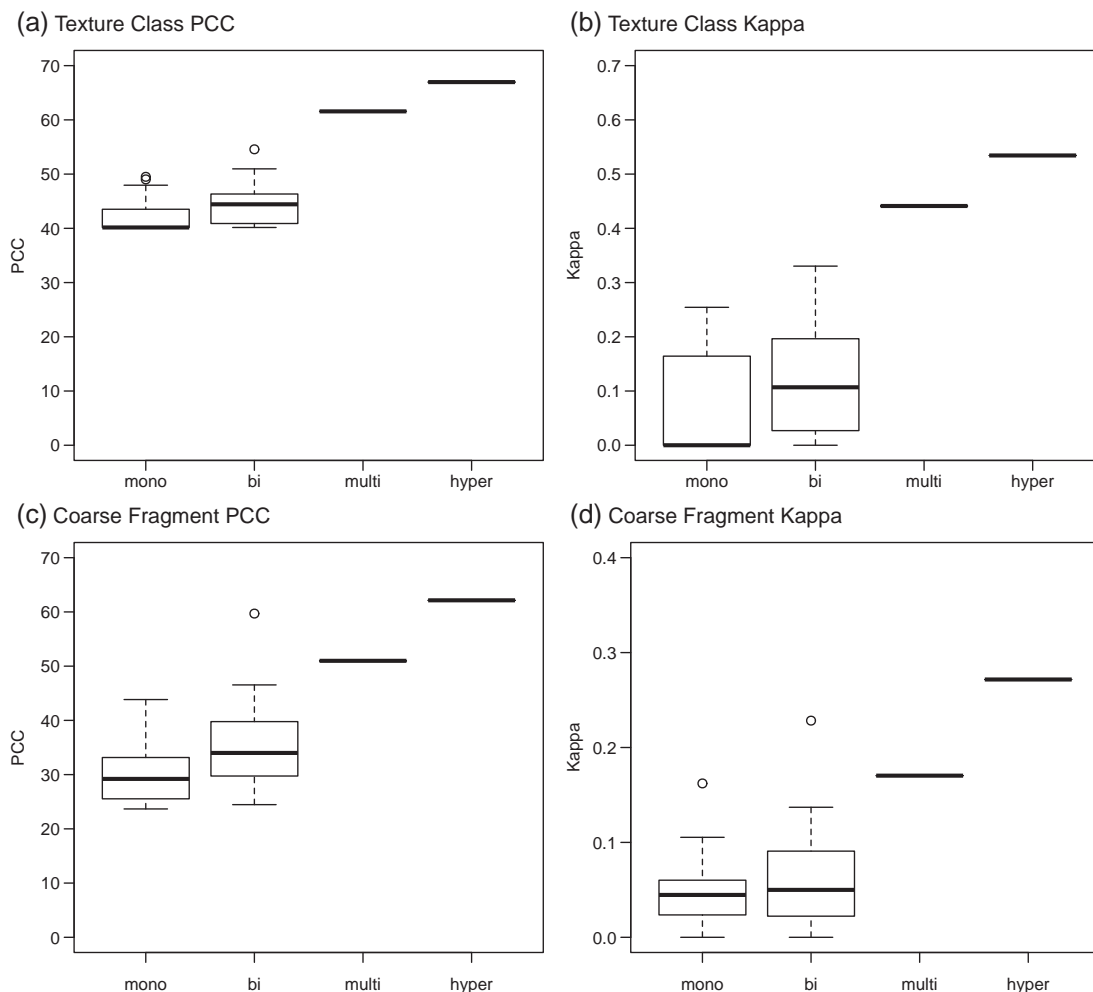


**Fig. 5.** Comparisons of soil texture class and coarse fragment class models using percent correctly classified (PCC) and Kappa for mono-temporal, bi-temporal, multi-temporal, and hyper-temporal SVM models.

**Table 2**  
Error matrix for hyper-temporal model of coarse fragment classes.

| Predictions | Class    | SVM error matrix |          |          |                  |
|-------------|----------|------------------|----------|----------|------------------|
|             |          | Reference        |          |          |                  |
|             |          | 0–14.9%          | 15–34.9% | 35–59.9% | UA% <sup>a</sup> |
|             | 0–14.9%  | 496              | 89       | 92       | 73               |
|             | 15–34.9% | 112              | 72       | 37       | 33               |
|             | 35–59.9% | 42               | 19       | 71       | 54               |
|             | PA%      | 76               | 40       | 36       | PCC = 62%        |
|             |          |                  |          |          | $\kappa = 0.27$  |

<sup>a</sup> UA is user's accuracy, PA is producer's accuracy, PCC is percent correctly classified,  $\kappa$  is kappa coefficient.

S2–S7. In general, producer's and user's accuracies for individual soil texture classes were similar, indicating the models' ability to both detect and predict sample classes with a similar level of accuracy. An exception to this trend is seen with the dominant soil texture class (SL), where user's accuracy decreased relative to producer's accuracies in models with decreasing temporal resolution (i.e., user's accuracy: mono- < bi- < multi- < hyper-temporal for SL) (Tables 1, S5–S7). This reflects the increasing over prediction of the dominant class in models with fewer significant NDVI covariates, reflecting models that are increasingly less robust. The soil texture classes with the lowest number of observations (i.e., SCL and L) had the lowest accuracies, while the soil texture class with the highest number of observations (i.e., SL) had the highest

accuracy. Model results for coarse fragment classes also showed similarities between producer's and user's accuracy, and in general, lower accuracies for under-sampled classes (i.e., 15–34.9%, 35–59.9%) (Tables 2, S5–S7). Model misclassification for hyper-temporal models represented by producer's accuracies and the number of misclassified predictions occurring in each adjacent class is shown in Table 1 and Fig. 6 for soil texture classes and Table 2 for coarse fragment classes.

5.4. Spatial predictions

Soil texture class predictions from SVM models showed varying degrees of association with parent materials and geomorphology in the study area, but the hyper-temporal model was the most effective in delineating patterns of textural classes that align with expected patterns from expert knowledge (Fig. 7). All four RS models indicate the widespread distribution of sandy loam textures, but the mono- and bi-temporal models (highest performing models for each type) predicted more sandy loam in the western portion of the study area than multi- or hyper-temporal models. Error matrices for mono- and bi-temporal models (Tables S2, S3) reveal the over prediction of the sandy loam class as reflected in the low user's accuracy relative to producer's accuracy. Additionally, the mono- and bi-temporal models were unable to predict all underrepresented classes, with only three classes predicted with the mono-temporal model and four classes predicted with the bi-temporal model. In contrast, multi- and hyper-temporal models predicted all six texture classes, demonstrating an increased ability to

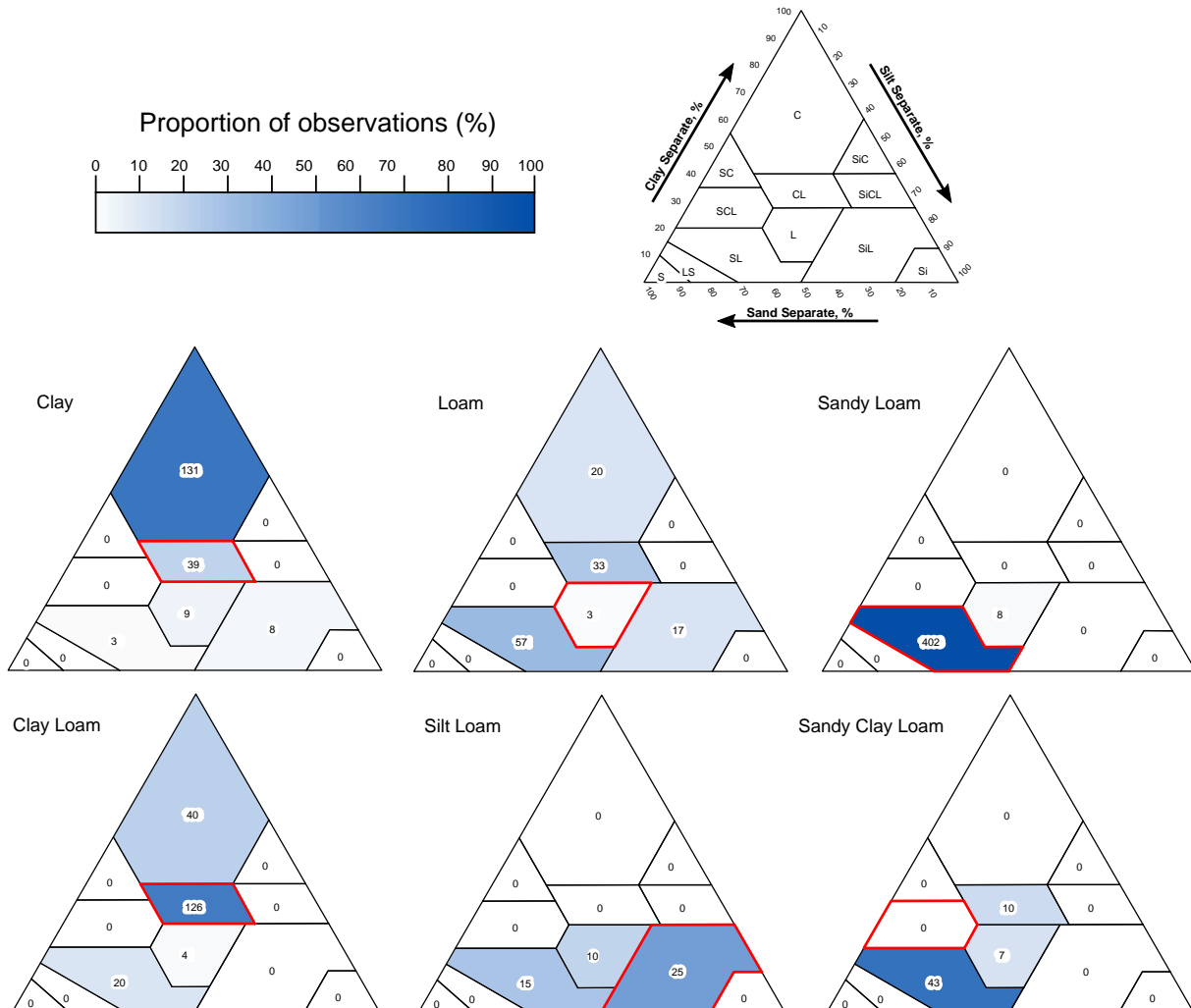


**Fig. 6.** Classification accuracy plots for individual textural classes illustrating the textural similarity in miss-classified observations.

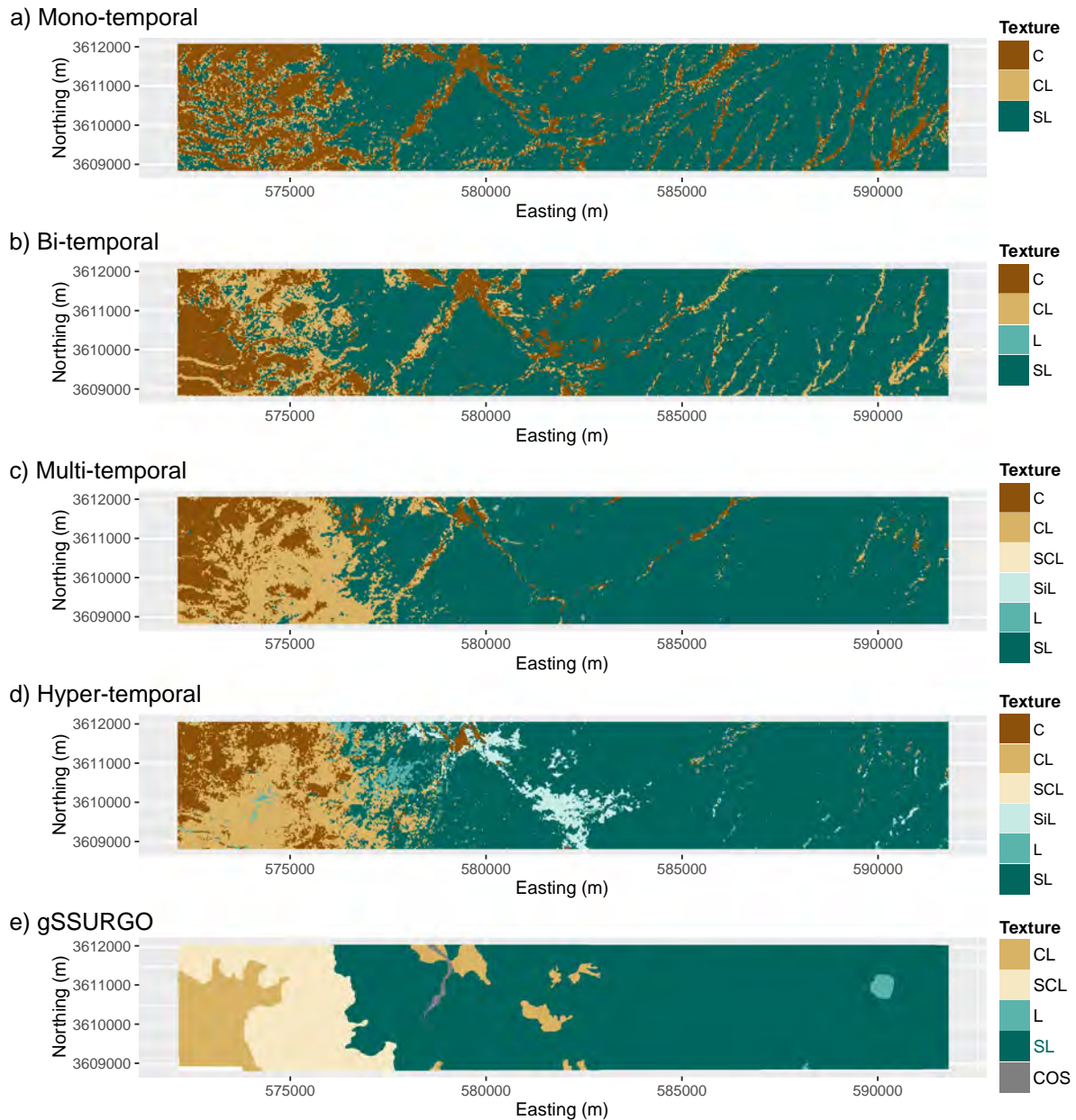


**Fig. 7.** Prediction maps of surface soil texture class for mono-temporal (a), bi-temporal (b), multi-temporal (c), hyper-temporal (d), SVM models and gSSURGO (e) aggregated by dominant condition.

model under sampled classes when the temporal frequency of covariate data increases. The hyper-temporal model, and to a lesser extent the multi-temporal model, predicted high clay content in soils of the western portion of the study area reflecting basalt and rhyolite parent material in contrast to the sandy alluvial deposits derived from granitic parent material in the eastern portion. Similarly, the hyper-temporal model predicted high silt content in bottomlands of the central portion of the study area which display patterns of the Miocene age lakebed sediments and the accumulation of fine materials in the lowest part of the landscape.

Similar to models of soil texture class, noticeable differences in coarse fragment class predictions can be seen across the four RS models (Fig. 8). Coarse fragment predictions from the mono-temporal model delineated many of the smaller drainages in the granitic alluvial fan in the eastern portion of the study area, but failed to predict the 35–

59.9% class. These drainages features are also visible in the bi-temporal model; however, the discontinuous prediction of the 35–59.9% class produced a ‘salt-and-pepper’ effect that masks many of the prominent landscape features. In contrast, the multi- and hyper-temporal models illustrated clear patterns of soil-landscape features and parent material differences. For example, the hyper-temporal model was effective in predicting the higher coarse fragment content in the volcanic parent materials located in the western half of the study area, whereas other models failed to predict these patterns.

Maps of gSSURGO texture and coarse fragment class, aggregated by dominant condition, were included to provide an external contextual reference for interpreting generalized spatial patterns of soil property classes. In general, a strong correspondence can be seen between the generalized gSSURGO maps and SVM model predictions.

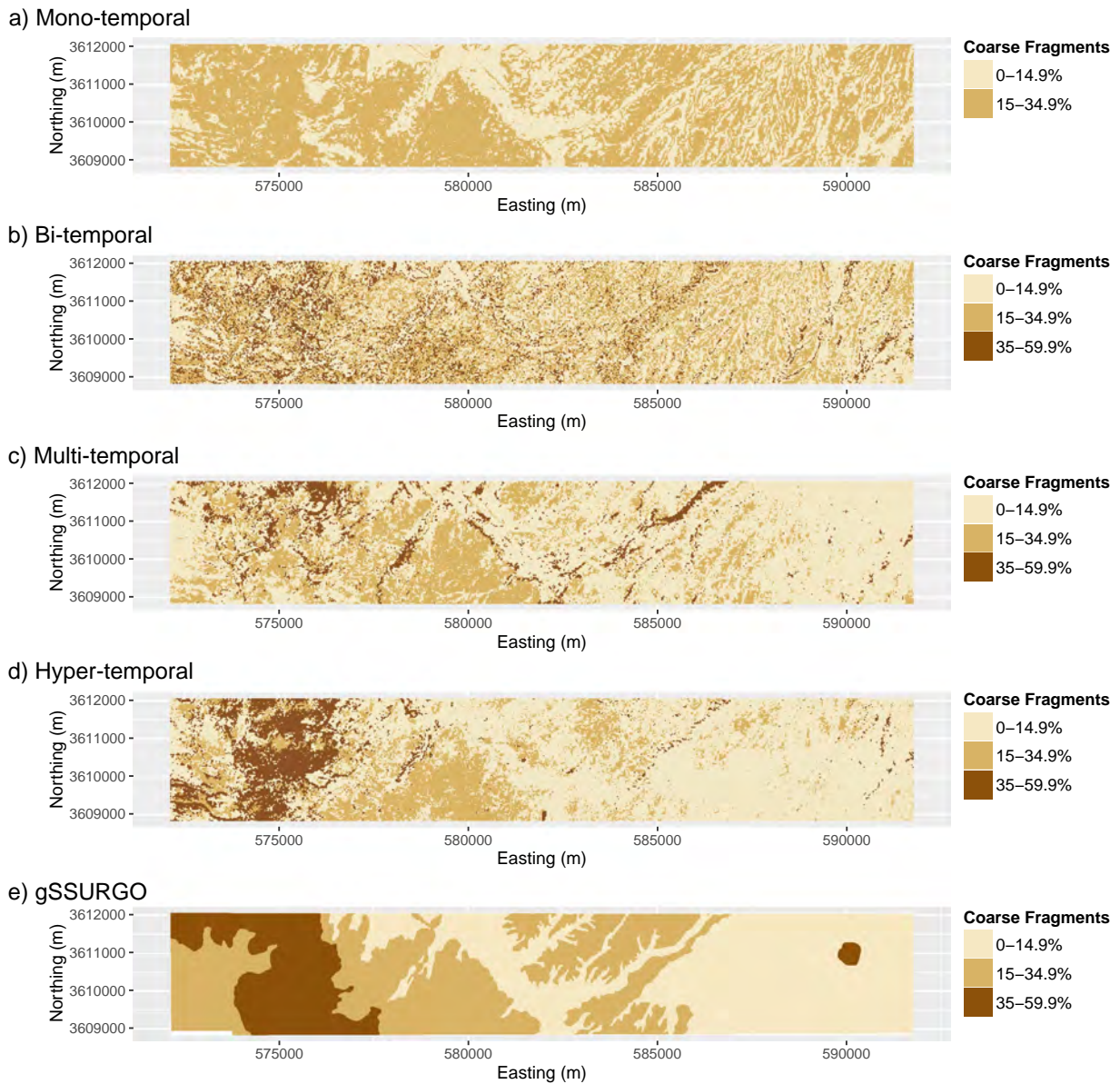


**Fig. 8.** Prediction maps of surface soil coarse fragment class for mono-temporal (a), bi-temporal (b), multi-temporal (c), hyper-temporal (d), SVM models and gSSURGO (e) aggregated by dominant condition.

**6. Discussion**

*6.1. Soil-climate-vegetation relationships*

In natural ecosystems, vegetation coexists with soil as part of a feedback system, where vegetation influences soil development, and in turn, the distribution of plant communities is influenced by soil physical and chemical properties (Ballabio et al., 2012). Within a landscape, the spatial distribution of soils and topography can create unique soil-climatic environments where only plant communities adapted to those conditions (i.e., ecological niche) can survive. This soil-vegetation feedback system results in predictable relationships between plant species composition and the soil properties that control its spatial distribution for a given climate. We have demonstrated that NDVI temporal response functions, extracted at each pixel location across the study area, were able to serve as a spectral ‘fingerprint’ of the soil with respect to soil texture and coarse fragment classes.

The controlling influence of soil properties on the distribution and dynamics of vegetation in semiarid landscapes has been well

documented (Levi et al., 2015; McAuliffe, 1994; Medeiros and Drezner, 2012; Michaud et al., 2013; Monger and Bestelmeyer, 2006; Parker, 2014). These relationships are largely controlled by available soil moisture and, to a lesser extent, chemical soil properties such as nutrient availability and pH. The ability to predict many soil properties is dependent upon identifying periods of variability in NDVI spectra that correspond to variation in the soil property of interest. Previous studies have shown that antecedent soil moisture can have a pronounced effect on net primary production (Reichmann et al., 2013; Sala et al., 2012) and the resulting spectral response of vegetation. For example, Levi et al. (2015) found that high antecedent moisture prior to monsoon rainfall in the Sonoran desert resulted in a reduced spectral response of vegetation during monsoon rainfall, particularly in years with dry monsoon conditions. Similar patterns were observed in this study, where transitions from dry to wet conditions, as identified from short-term SPI, show amplified NDVI spectral response. These periods are also characterized by high variability in NDVI. For example, many of the significant image dates within our texture class SVM occurred during transitions between periods of extreme drought and abnormal

wetness (e.g., September–November 2006), which are associated with concomitant peaks in NDVI and NDVI spectral variability (Fig. 4). Our results show, however, that spectral variability resulting from transitions in climate are not restricted to dry-to-wet transitions, but rather occur during transitions between all climatic states (i.e., wet-to-dry) (Fig. 4). Variability in the amplitude of inter-annual NDVI and NDVI SD at peak biomass was related to variability in short-term SPI which characterized transitions between climatic states. Furthermore, the effect of long-term precipitation anomalies (i.e., SPI 20–36 months) drives the frequency of high variability transition events (Fig. 4). In general, periods along the time series that characterize the most dramatic transitions between climatic states corresponded to the significant scenes within our SVM models.

## 6.2. Soil property predictions

Results from this study showed that increasing the temporal frequency of RS imagery used in soil prediction models can greatly improve the accuracy of model predictions (Fig. 5). Furthermore, this study showed that these improvements were the result of a more resolved characterization of soil-vegetation dynamics and the temporal variability that emerges from climatic feedbacks. As a result, soil prediction models that utilize hyper-temporal RS may have a significant advantage over models using mono-, bi-, or multi-temporal RS imagery. However, the improved ability of hyper-temporal RS to predict soil properties, relative to traditional RS approaches, is dependent upon how direct of an influence the soil property has on vegetation dynamics. Soil texture exerts a primary or direct control on vegetation spectra, and thus produced a high PCC and  $\kappa$  for the hyper-temporal model. In contrast, coarse fragment content has a much weaker influence on vegetation spectra, and while it produced a comparable PCC, it had a much lower  $\kappa$  value for the hyper-temporal model. In addition to the fundamental strength of the predictor-response relationship, several other factors influence model predictions, including: (i), the frequency distribution of sample classes, and (ii) the number of classes being predicted and their degree of similarity with respect to model covariates.

The unbalanced frequency class distribution for texture and coarse fragments is likely a result of both our sampling strategy and the spatial distribution of sample classes within our study area. Approximately half of our sample locations were selected using cLHS, a sampling method that randomly stratifies sampling locations across feature space, thus representing the multivariate distribution of input environmental covariates. The environmental covariates used in the cLHS were based on a previous study that included both topographic and RS indices. While the use of this sampling strategy likely captured much of the spectral variability present in the hyper-temporal NDVI image time series, a cLHS based directly on the hyper-temporal image stack may have potentially improved the class distribution and overall model accuracy. The remaining half of our samples were NRCS field transects, where sampling locations were purposive and selected based on expert knowledge. This type of sampling approach is more likely to result in the underrepresentation of uncommon sample classes. Thus in highly complex and heterogeneous landscapes, if the initial sampling design fails to adequately account for the spatial distribution of sample classes, the less common sample classes will tend to be underrepresented as was the case in this study.

The interpretation of model misclassification for categorical data depends upon the types of relationships that exist between classes. For example, coarse fragment classes exhibit a linear relationship where each class increases in its percentage of coarse fragments, thus any coarse fragment class is at most directly related to only two adjacent classes (i.e., greater than and/or less than specified range). In contrast, soil textural classes are related in two dimensional space based upon a specified range of sand, silt, and clay content. Consequently, many different textural classes can reside in close textural space to any one soil texture class. This more complex relationship between texture classes

makes the interpretation of model misclassification more complicated. By examining model misclassification results for texture classes using textural triangles, we can visualize where the misclassified values fall in textural space relative to their actual class (Fig. 6). For example, the sandy clay loam class had a producer's accuracy of 0%, meaning that no clay loam class observations were correctly classified. However, upon further examination we see that all of the sandy clay loam observations were misclassified to similar, adjacent texture classes; with 72, 17, and 12% classified as sandy loam, clay loam, and loam, respectively (Fig. 6). Sandy loam was the dominant texture class in the study area and 98% of the samples were correctly classified. The disproportionately large number of samples representing sandy loam likely explains why many of the misclassified samples in neighboring texture classes (i.e., loam, silt loam, sandy clay loam) were predicted as sandy loam. The misclassification of soil texture classes to adjacent texture classes is not surprising given the similar biophysical response these related texture classes can exert on ecosystem structure and function.

## 6.3. Spatial patterns of soil texture and coarse fragment classes

While all RS models predicted similar generalized landscape patterns, they differed strongly in their ability to predict all soil classes, as well as to provide predictions that align with known spatial patterns of parent materials and geomorphic features. For example, the western portion of the study area is dominated by basalt hills and rhyolitic alluvial fans that produce fine textured soils. The mono-temporal model, and to a lesser extent the bi-temporal model, predicted substantial areas of sandy loam in this region. In contrast, the multi- and hyper-temporal models predicted predominantly clay and clay loam textures which align with our expectations. Additionally, the dominant influence of maximum annual NDVI in both the mono- and bi-temporal models resulted in spatial patterns of soil classes that highlight areas with high vegetative cover. For example, the primary drainage in the center of the study area has dense cover of *S. wrightii* along with other shrubs and trees; and the smaller drainages dissecting the granitic alluvial fan in the eastern portion of the study area characterized by dense stands of *Prosopis* spp. These patterns are less prominent in the multi- and hyper-temporal models because they represented more of the inter-annual variability of vegetation patterns. Spatial predictions of soil texture from the hyper-temporal model corresponded well with generalized texture patterns from gSSURGO, with the exception of sections of the western portion of the study area where gSSURGO fails to accurately represent the clay texture class. Additionally, we should note that the mono-temporal and bi-temporal model predictions presented in Figs. 7 and 8 represent best-case scenarios, that is, they represent the strongest of the 28 models of each model type. In many cases both the mono- and bi-temporal models had no predictive ability, assigning all observations to the dominant class. Consequently, when utilizing a mono- or bi-temporal model, the chance of obtaining a meaningful outcome is highly variable.

Spatial predictions of soil coarse fragment classes showed that as the temporal frequency of model covariates increased, there was an increased ability to differentiate the geomorphic features and parent materials that control the distribution of coarse fragments across the study area. Similar to soil texture class predictions, the mono-temporal model of coarse fragments represents peak vegetation which may explain why the patterns of the primary drainage were so discrete compared to the upland landscapes with less vegetative cover. Poor representation of spatial patterns in the bi-temporal model likely reflect the contrasting vegetative patterns during wet and dry conditions, as this model was developed with peak and non-peak NDVI. Improved spatial predictions of coarse fragment classes can be seen in the multi- and hyper-temporal models, with the hyper-temporal model producing spatial patterns that correspond most closely to expected distributions. Additionally, spatial predictions from the hyper-temporal model were the most similar to

that of gSSURGO and highlight the majority of the landscape patterns discernable in gSSURGO.

#### 6.4. Future applications of hyper-temporal remote sensing for soil mapping

In this study we demonstrate the ability of hyper-temporal RS to characterize the soil-vegetation relationship and its response to climatic variability in arid and semi-arid ecosystems; and the utility of using the spectral response resulting from these soil-vegetation dynamics for predicting soil properties. While few studies have developed soil proxies from vegetation cover, one approach has been to associate soil properties with plant functional types (PFT), which represent broad groupings of vegetation based on similarities in morphological and physiological traits constrained by environmental resources and conditions (Ustin and Gamon, 2010). Prior efforts to map PFT using remote sensing have employed a static or mono-temporal approach (Buis et al., 2009; Schaepman et al., 2007; Ustin and Gamon, 2010), and while these efforts are useful in characterizing soil-vegetation spatial variation (Ballabio et al., 2012), growing evidence supports the notion that temporal variability in vegetation spectra, as driven by soil and climate feedbacks, is an important predictor of soil variability. Since environmental resources and conditions change in response to internal and external drivers, the morphological and physiological traits expressed by PFTs will also change. Our approach builds upon the concept of PFT, but further extends this concept to include temporal variability in vegetation spectra relating to internal and external drivers, thus allowing the development of a spectral ‘fingerprint’ of the soil-vegetation relationship.

Although few studies have employed a hyper-temporal RS approach for DSM, previous studies using a multi-temporal approach have demonstrated the potential utility of characterizing soil-vegetation temporal response for mapping a variety of soil properties (see Table S1). The extent to which RS temporal response functions can predict specific soil properties or classes depends on the biophysical or biochemical relationships that exist between vegetation properties detectable via RS and the soil property of interest. A wide variety of soil properties can be linked to individual vegetation indices; however, more complete temporal response functions appear to be more robust for modeling soil properties that either exert a direct control on vegetation patterns or those properties that are directly influenced by vegetation dynamics. This is in contrast to those soil properties that are indirectly tied to the spectral response of vegetation through time and space.

Although not examined in this study, terrain attributes are some of the most commonly used covariates for predicting soil properties (Grunwald, 2009; McBratney et al., 2003). Terrain attributes and spectral indices often exhibit considerable cross correlation due to the strong interrelationships between factors in the soil environment. Nonetheless, previous studies have shown that the combination of both terrain and RS data produces the most accurate classifications of soils in complex geomorphic landscapes (Dobos et al., 2000; Ehsani and Quiel, 2009; Martin and Franklin, 2005; Taramelli and Meelli, 2009), indicating that terrain and spectral indices each possess some unique amount of explanatory power. Future research is needed to examine the added benefit of incorporating both hyper-temporal RS and terrain attributes into soil prediction models.

## 7. Conclusion

In this study we have reviewed and synthesized, through the lens of temporal variability, previous research utilizing RS imagery for DSM. Results from this review showed that the majority of DSM studies that use RS have employed a mono-temporal RS methodology, and that these mono-temporal RS covariates have been important predictors in DSM models. However, growing evidence supports the notion that temporal variability in vegetation spectra, as driven by soil and climate feedbacks, is an important predictor of soil variability. This recognition,

combined with the removal of prior constraints (e.g., imagery cost, computational efficiency) on using high frequency RS time series in DSM, has led to the increasing use of multi- and hyper-temporal RS in DSM in recent years.

In this study, we demonstrated the efficacy of the hyper-temporal RS approach in predicting soil texture and coarse fragment classes in a semiarid region of the southwestern United States. We highlight how hyper-temporal RS can improve current methods of soil mapping efforts due to its ability to characterize both intra- and inter-annual variability at a high temporal resolution, allowing the detection of subtle changes in RS spectra relating to variation in soil properties. The hyper-temporal models outperformed the mono-, bi-, and multi-temporal models that represented more traditional approaches for incorporating RS data in DSM models. Furthermore, this study showed that in the majority of cases, mono- and bi-temporal models produced spurious results due to suboptimal timing of image selection. In these arid ecosystems, hyper-temporal RS was highly effective in modeling soil texture due to its direct control on vegetation spectral variability in response to climatic variability. Coarse fragment class was also effectively modeled, although with a weaker model relative to soil texture. Our results show that short-term precipitation patterns (i.e., short-term SPI) were driving variability in the amplitude of inter-annual NDVI and resulting SD of NDVI at peak biomass. Furthermore, our analysis showed that long-term precipitation anomalies (long-term drought, long-term wetness) drive the frequency of these high variability transition events. In general, the periods along the time series that characterize the most dramatic transitions between climatic states correspond to the significant scenes within our SVM models. Consequently, the optimal time-series for modeling soil properties is not dependent upon its length, but rather that it encompasses a time period that includes a range of climatic extremes which results in maximized spectral variability. The hyper-temporal RS approach can improve current DSM efforts for a range of soil properties and classes; however, additional research is needed to test the efficacy of the hyper-temporal approach for other soil properties and in other ecosystems and environments.

## Acknowledgements

This work was supported by the USDA ARS Postdoctoral Research Associate Program, the USDA-NRCS of Arizona cooperative agreement 68-9457-8-466 NSF EAR/IF #0929850, and the Arizona Agricultural Experiment Station ARZT-1367190-H21-155. We also thank three anonymous reviewers for comments that improved this manuscript.

## Appendix A. Supplementary data

Supplementary data to this article can be found online at <http://dx.doi.org/10.1016/j.geoderma.2016.09.024>.

## References

- Adegoke, J.O., Carleton, A.M., 2002. Relations between soil moisture and satellite vegetation indices in the U.S. Corn Belt. *J. Hydrometeorol.* 3, 395–405.
- Anderson, G., Hanson, J., Haas, R., 1993. Evaluating landsat thematic mapper derived vegetation indices for estimating above-ground biomass on semiarid rangelands. *Remote Sens. Environ.* 45, 165–175.
- Araya, S., Lyle, G., Lewis, M., Ostendorf, B., 2016. Phenologic metrics derived from MODIS NDVI as indicators for Plant Available Water-holding Capacity. *Ecol. Indic.* 60, 1263–1272.
- Bachofer, F., Quéhérvé, G., Hochschild, V., Maerker, M., 2015. Multisensoral topsoil mapping in the semiarid lake Manyara Region, Northern Tanzania. *Remote Sens.* 7, 9563–9586.
- Ballabio, C., Fava, F., Rosenmund, A., 2012. A plant ecology approach to digital soil mapping, improving the prediction of soil organic carbon content in alpine grasslands. *Geoderma* 187–188, 102–116.
- Basnyat, P., McConkey, B.G., Selles, F., Meinert, L.B., 2005. Effectiveness of using vegetation index to delineate zones of different soil and crop grain production characteristics. *Can. J. Soil Sci.* 85, 319–328.
- Ben-Dor, E., Taylor, R.C., Hill, J., Dematté, J.A.M., Whiting, M.L., Chabrilat, S., Sommer, S., 2008. Imaging spectrometry for soil applications. *Adv. Agron.* 97, 321–392.

- Blasch, G., Spengler, D., Hohmann, C., Neumann, C., Itzerott, S., Kaufmann, H., 2015. Multitemporal soil pattern analysis with multispectral remote sensing data at the field-scale. *Comput. Electron. Agric.* 113, 1–13.
- Boettinger, J.L., Ramsey, R.D., Bodily, J.M., Cole, N.J., Nield, S.J., Saunders, A.M., Stum, A.K., 2008. Landsat spectral data for digital soil mapping. *Digital Soil Mapping With Limited Data*, pp. 193–202.
- Brown, D.E., 1982. *Biotic Communities: Southwestern United States and Northwestern Mexico*. University of Utah Press.
- Brown, D.E., Lowe, C.H., 1978. *Biotic Communities of the Southwest*. Rocky Mountain Forest and Range Experiment Station, USDA Forest Service.
- Brungard, C.W., Boettinger, J.L., Duniway, M.C., Wills, S.a., Edwards, T.C., 2015. Machine learning for predicting soil classes in three semi-arid landscapes. *Geoderma* 239–240, 68–83.
- Buis, E., Veldkamp, A., Boeken, B., Breemen, N.V., 2009. Controls on plant functional surface cover types along a precipitation gradient in the Negev Desert of Israel. *J. Arid Environ.* 73, 82–90.
- Casady, G.M., van Leeuwen, W.J.D., Reed, B.C., 2013. Estimating winter annual biomass in the Sonoran and Mojave Deserts with satellite- and ground-based observations. *Remote Sens.* 5, 909–926.
- Chagas, C. da S., Vieira, C.A.O., Fernandes Filho, E.I., 2013. Comparison between artificial neural networks and maximum likelihood classification in digital soil mapping. *Rev. Bras. Ciênc. Solo* 37 (2), 339–351.
- Cleveland, R.B., Cleveland, W.S., McRae, J.E., Terpenning, I., 1990. STL: a seasonal-trend decomposition procedure based on loess. *J. Off. Stat.* 6, 3–73.
- Congalton, R.G., Green, K., 2008. *Assessing the Accuracy of Remotely Sensed Data: Principles and Practices*. CRC press.
- Core Team, R., 2015. *R: A Language and Environment for Statistical Computing*. R Found. Stat. Comput (ISBN).
- Dobos, E., Micheli, E., Baumgardner, M.F., Biehl, L., Helt, T., 2000. Use of combined digital elevation model and satellite radiometric data for regional soil mapping. *Geoderma* 97, 367–391.
- Dobos, E., Montanarella, L., Nègre, T., Micheli, E., 2001. A regional scale soil mapping approach using integrated AVHRR and DEM data. *Int. J. Appl. Earth Obs. Geoinf.* 3, 30–42.
- Dutta, D., Goodwell, A.E., Kumar, P., Garvey, J.E., Darmody, R.G., Berretta, D.P., Greenberg, J.A., 2015. On the feasibility of characterizing soil properties from AVIRIS data. *IEEE Trans. Geosci. Remote Sens.* 53, 5133–5147.
- Ehsani, A.H., Quiel, F., 2009. A semi-automatic method for analysis of landscape elements using Shuttle Radar Topography Mission and Landsat ETM+ data. *Comput. Geosci.* 35, 373–389.
- Farrar, T.J., Nicholson, S.E., Lare, A.R., 1994. The influence of soil type on the relationships between NDVI, rainfall, and soil-moisture in semiarid Botswana. 2. NDVI response to soil-moisture. *Remote Sens. Environ.* 50, 121–133.
- Gao, X., Huete, A.R., Ni, W., Miura, T., 2000. Optical-biophysical relationships of vegetation spectra without background contamination. *Remote Sens. Environ.* 74, 609–620.
- Gibbens, R.P., McNeely, R.P., Havstad, K.M., Beck, R.F., Nolen, B., 2005. Vegetation changes in the Jornada Basin from 1858 to 1998. *J. Arid Environ.* 61, 651–668.
- Grunwald, S., 2009. Multi-criteria characterization of recent digital soil mapping and modeling approaches. *Geoderma* 152, 195–207.
- Grunwald, S., Vasques, G.M., Rivero, R.G., 2015. Fusion of soil and remote sensing data to model soil properties. *Adv. Agron.* 131, 1–109.
- Hansen, M.C., Potapov, P.V., Moore, R., Hancher, M., Turubanova, S.A., Tyukavina, A., Thau, D., Stehman, S.V., Goetz, S.J., Loveland, T.R., Kommareddy, A., Egorov, A., Chini, L., Justice, C.O., Townshend, J.R.G., 2013. High-resolution global maps of 21st-century forest cover change. *Science* 342, 850–853.
- Henderson, B.L., Bui, E.N., Moran, C.J., Simon, D.A.P., 2005. Australia-wide predictions of soil properties using decision trees. *Geoderma* 124, 383–398.
- Hengl, T., Rossiter, D.G., Stein, A., 2003. Soil sampling strategies for spatial prediction by correlation with auxiliary maps. *Aust. J. Soil Res.* 41, 1403–1422.
- Heung, B., Ho, H.C., Zhang, J., Knudby, A., Bulmer, C.E., Schmidt, M.G., 2016. An overview and comparison of machine-learning techniques for classification purposes in digital soil mapping. *Geoderma* 265, 62–77.
- Huete, A., 1988. A soil-adjusted vegetation index (SAVI). *Remote Sens. Environ.* 25, 295–309.
- Jackson, M.L., 2005. *Soil Chemical Analysis: Advanced Course*. UW-Madison Libraries Parallel Press.
- Jenerette, G.D., Scott, R.L., Huete, A.R., 2010. Functional differences between summer and winter season rain assessed with MODIS-derived phenology in a semi-arid region. *J. Veg. Sci.* 21, 16–30.
- Kawamura, K., Akiyama, T., Yokota, H.O., Tsutsumi, M., Yasuda, T., Watanabe, O., Wang, S., 2005. Quantifying grazing intensities using geographic information systems and satellite remote sensing in the Xilingol steppe region, Inner Mongolia, China. *Agric. Ecosyst. Environ.* 107, 83–93.
- Kennedy, R.E., Andréfouët, S., Cohen, W.B., Gómez, C., Griffiths, P., Hais, M., Healey, S.P., Helmer, E.H., Hostert, P., Lyons, M.B., Meigs, G.W., Pflugmacher, D., Phinn, S.R., Powell, S.L., Scarth, P., Sen, S., Schroeder, T.a., Schneider, A., Sonnenschein, R., Vogelmann, J.E., Wulder, M.a., Zhu, Z., 2014. Bringing an ecological view of change to landsat-based remote sensing. *Front. Ecol. Environ.* 12, 339–346.
- Kerr, J.T., Ostrovsky, M., 2003. From space to species: ecological applications for remote sensing. *Trends Ecol. Evol.* 18, 299–305.
- Kuhn, M., 2008. Building predictive models in R using the caret package. *J. Stat. Softw.* 28, 1–26.
- Kuhn, M., Johnson, K., 2013. *Applied Predictive Modeling*. Springer.
- Kunkel, M.L., Flores, A.N., Smith, T.J., McNamara, J.P., Benner, S.G., 2011. A simplified approach for estimating soil carbon and nitrogen stocks in semi-arid complex terrain. *Geoderma* 165, 1–11.
- Kurc, S.A., Benton, L.M., 2010. Digital image-derived greenness links deep soil moisture to carbon uptake in a creosotebush-dominated shrubland. *J. Arid Environ.* 74, 585–594.
- Levi, M.R., Rasmussen, C., 2014. Covariate selection with iterative principal component analysis for predicting physical soil properties. *Geoderma* 219–220, 46–57.
- Levi, M.R., Schaap, M.G., Rasmussen, C., 2015. Application of spatial pedotransfer functions to understand soil modulation of vegetation response to climate. *Vadose Zo.* 14.
- Li, Z., Huffman, T., Zhang, A., Zhou, F., McConkey, B., 2012. Spatially locating soil classes within complex soil polygons - mapping soil capability for agriculture in Saskatchewan Canada. *Agric. Ecosyst. Environ.* 152, 59–67.
- Lozano-Garcia, D.F., Fernandez, R.N., Johannsen, C.J., 1991. Assessment of regional biomass-soil relationships using vegetation indexes. *IEEE Trans. Geosci. Remote Sens.* 29, 331–339.
- Main-Knorn, M., Cohen, W.B., Kennedy, R.E., Grodzki, W., Pflugmacher, D., Griffiths, P., Hostert, P., 2013. Monitoring coniferous forest biomass change using a Landsat trajectory-based approach. *Remote Sens. Environ.* 139, 277–290.
- Martin, Y.E., Franklin, S.E., 2005. Classification of soil and bedrock dominated landslides in British Columbia using segmentation of satellite imagery and DEM data. *Int. J. Remote Sens.* 26, 1505–1509.
- Masek, J.G., Vermote, E.F., Saleous, N.E., Wolfe, R., Hall, F.G., Huemmrich, K.F., Gao, F., Kutler, J., Lim, T.K., 2006. A landsat surface reflectance dataset for North America, 1990–2000. *IEEE Geosci. Remote Sens. Lett.* 3, 68–72.
- McAuliffe, J., 1994. Landscape evolution, soil formation, and ecological patterns and processes in Sonoran Desert bajadas. *Ecol. Monogr.* 64, 111–148.
- McBratney, A.B., Santos, M.L.M., Minasny, B., 2003. On digital soil mapping. *Geoderma* 117, 3–52.
- McKee, T.B., Doesken, N.J., Kleist, J., 1993. The relationship of drought frequency and duration to time scales. *AMS 8th Conf. Appl. Climatol.*, pp. 179–184.
- Medeiros, A.S., Drezner, T.D., 2012. Vegetation, climate, and soil relationships across the Sonoran Desert. *Ecoscience* 19, 148–160.
- Melton, M.A., 1965. The geomorphic and paleoclimatic significance of alluvial deposits in southern Arizona. *J. Geol.* 1–38.
- Michaud, G.A., Monger, H.C., Anderson, D.L., 2013. Geomorphic-vegetation relationships using a geopedological classification system, northern Chihuahuan Desert, USA. *J. Arid Environ.* 90, 45–54.
- Minasny, B., McBratney, A.B., 2006. A conditioned Latin hypercube method for sampling in the presence of ancillary information. *Comput. Geosci.* 32, 1378–1388.
- Mohanty, B.P., 2013. Soil hydraulic property estimation using remote sensing: a review. *Vadose Zo. J.* 12.
- Monger, H.C., Bestelmeyer, B.T., 2006. The soil-geomorphic template and biotic change in arid and semi-arid ecosystems. *J. Arid Environ.* 207–218.
- Mulder, V.L., de Bruin, S., Schaeppman, M.E., Mayr, T.R., 2011. The use of remote sensing in soil and terrain mapping - a review. *Geoderma* 162, 1–19.
- Nawar, S., Buddenbaum, H., Hill, J., 2015. Digital mapping of soil properties using multivariate statistical analysis and ASTER data in an arid region. *Remote Sens.* 7, 1181–1205.
- Nield, S.J., Boettinger, J.L., Ramsey, R.D., 2007. Digitally mapping gypsic and natric soil areas using Landsat ETM data. *Soil Sci. Soc. Am. J.* 71, 245.
- Omuto, C.T., Shrestha, D.P., 2007. Remote sensing techniques for rapid detection of soil physical degradation. *Int. J. Remote Sens.* 28, 4785–4805.
- Page, K.L., Dalal, R.C., Pringle, M.J., Bell, M., Dang, Y.P., Radford, B., Bailey, K., 2013. Organic carbon stocks in cropping soils of Queensland, Australia, as affected by tillage management, climate, and soil characteristics. *Soil Res.* 51, 596–607.
- Parker, K.C., 2014. Topography, substrate, and vegetation patterns in the northern Sonoran Desert. *J. Biogeogr.* 18, 151–163.
- Peng, Y., Xiong, X., Adhikari, K., Knadel, M., Grunwald, S., Greve, M.H., 2015. Modeling soil organic carbon at regional scale by combining multi-spectral images with laboratory spectra. *PLoS One* 10, 1–22.
- Poggio, L., Gimona, A., Brewer, M.J., 2013. Regional scale mapping of soil properties and their uncertainty with a large number of satellite-derived covariates. *Geoderma* 209–210, 1–14.
- PRISM Climate Group, 2008. Oregon State University. <http://www.prism.oregonstate.edu/>, created 31 Oct 2008.
- Purevdorj, T., Tateishi, R., Ishiyama, T., Honda, Y., 1998. Relationships between percent vegetation cover and vegetation indices. *Int. J. Remote Sens.* 19, 3519–3535.
- Rad, M.R.P., Toomanian, N., Khormali, F., Brungard, C.W., Komaki, C.B., Bogaert, P., 2014. Updating soil survey maps using random forest and conditioned Latin hypercube sampling in the loess derived soils of northern Iran. *Geoderma* 232, 97–106.
- Reichmann, L.G., Sala, O.E., Peters, D.P.C., 2013. Precipitation legacies in desert grassland primary production occur through previous-year tiller density. *Ecology* 94, 435–443.
- Reynolds, S.J., Richard, S.M., Spencer, J.E., Pearthree, P.A., 2000. *Geologic Map of Arizona*. Arizona Geological Survey.
- Richardson, A.J., Wiegand, C.L., 1977. Distinguishing vegetation from soil background information. *Photogramm. Eng. Remote. Sens.* 43, 1543–1551.
- Rivero, R., Grunwald, S., Bruland, G., 2007. Incorporation of spectral data into multivariate geostatistical models to map soil phosphorus variability in a Florida wetland. *Geoderma* 140, 428–443.
- Sala, O., Parton, W., Joyce, L., Lauenroth, W., 1988. Primary production of the central grassland region of the United States. *Ecology* 69, 40–45.
- Sala, O.E., Gherardi, L.A., Reichmann, L., Jobbágy, E., Peters, D., 2012. Legacies of precipitation fluctuations on primary production: theory and data synthesis. *Philos. Trans. R. Soc. Lond. Ser. B Biol. Sci.* 367, 3135–3144.
- Sala, O.E., Gherardi, L.A., Peters, D.P.C., 2015. Enhanced precipitation variability effects on water losses and ecosystem functioning: differential response of arid and mesic regions. *Clim. Chang.* 213–227.

- Sankey, T.T., Weber, K.T., 2009. Rangeland assessments using remote sensing: is NDVI useful? Final Report: Comparing Effects of Management Practices on Rangeland Health With Geospatial Technologies (NNX06AE47G), p. 168
- Schaepman, M.E., Wamelink, G.W.W., Dobben, H.F.V., Gloor, M., 2007. River floodplain vegetation scenario development using imaging spectroscopy derived products as input variables in a dynamic vegetation model. *Photogramm. Eng. Remote. Sens.* 73, 1179–1188.
- Schmidt, H., Karnieli, A., 2000. Remote sensing of the seasonal variability of vegetation in a semi-arid environment. *J. Arid Environ.* 45, 43–59.
- Schnur, M.T., Xie, H., Wang, X., 2010. Estimating root zone soil moisture at distant sites using MODIS NDVI and EVI in a semi-arid region of southwestern USA. *Ecol. Inform.* 5, 400–409.
- Scull, P., Franklin, J., Chadwick, O.a., McArthur, D., 2003. Predictive soil mapping: a review. *Prog. Phys. Geogr.* 27, 171–197.
- Shabou, M., Mougnot, B., Chabaane, Z., Walter, C., Boulet, G., Aissa, N., Zribi, M., 2015. Soil clay content mapping using a time series of Landsat TM data in semi-arid lands. *Remote Sens.* 7, 6059–6078.
- Shepard, C., Schaap, M.G., Crimmins, M.a., van Leeuwen, W.J.D., Rasmussen, C., 2015. Sub-surface soil textural control of aboveground productivity in the US Desert Southwest. *Geoderma Reg.* 4, 44–54.
- Sheppard, P., Comrie, A., Packin, G.D., Angersbach, K., Hughes, M., 2002. The climate of the US Southwest. *Clim. Res.* 21, 219–238.
- Soil Survey Staff, 2011. Soil Survey of Graham County, Arizona, Southwestern Part.
- Soil Survey Staff, 2015. Gridded Soil Survey Geographic (gSSURGO) Database for Arizona.
- Sponseller, R.A., Hall, S.J., Huber, D.P., Grimm, N.B., Kaye, J.P., Clark, C.M., Collins, S.L., 2012. Variation in monsoon precipitation drives spatial and temporal patterns of *Larrea tridentata* growth in the Sonoran Desert. *Funct. Ecol.* 26, 750–758.
- Taghizadeh-Mehrjardi, R., Nabiollahi, K., Minasny, B., Triantafyllis, J., 2015. Comparing data mining classifiers to predict spatial distribution of USDA-family soil groups in Baneh region, Iran. *Geoderma* 253–254, 67–77.
- Taramelli, A., Melelli, L., 2009. Map of deep seated gravitational slope deformations susceptibility in central Italy derived from SRTM DEM and spectral mixing analysis of the Landsat ETM+ data. *Int. J. Remote Sens.* 30, 357–387.
- Twarakavi, N.K.C., Šimůnek, J., Schaap, M.G., 2009. Development of pedotransfer functions for estimation of soil hydraulic parameters using support vector machines. *Soil Sci. Soc. Am. J.* 73, 1443.
- Ustin, S.L., Gamon, J.a., 2010. Remote sensing of plant functional types. *New Phytol.* 186, 795–816.
- Verbesselt, J., Hyndman, R., Newnham, G., Culvenor, D., 2010. Detecting trend and seasonal changes in satellite image time series. *Remote Sens. Environ.* 114, 106–115.
- Walker, D.A., Jia, G.J., Epstein, H.E., Reynolds, M.K., Chapin, I.S., Copass, C., Hinzman, L.D., Knudson, J.A., Maier, H.A., Michaelson, G.J., Nelson, F., Ping, C.L., Romanovsky, V.E., Shiklomanov, N., 2003. Vegetation-soil-thaw-depth relationships along a low-arctic bioclimate gradient, Alaska: synthesis of information from the ATLAS studies. *Permafrost. Periglacial Process.* 14, 103–123.
- Wang, X., Xie, H., Guan, H., Zhou, X., 2007. Different responses of MODIS-derived NDVI to root-zone soil moisture in semi-arid and humid regions. *J. Hydrol.* 340, 12–24.
- Williamson, J.C., Bestelmeyer, B.T., Peters, D.P.C., 2012. Spatiotemporal patterns of production can be used to detect state change across an arid landscape. *Ecosystems* 15, 34–47.
- Wilson, E.D., Moore, R.T., 1958. Geologic Map of Graham and Greenlee Counties, Arizona. Arizona Bur. Mines, Univ. of Arizona.
- Woodcock, C.E., Allen, R., Anderson, M., Belward, A., Bindschadler, R., Cohen, W., Gao, F., Goward, S.N., Helder, D., Helmer, E., Nemani, R., Oreopoulos, L., Schott, J., Thenkabail, P.S., Vermote, E.F., Vogelmann, J., Wulder, M.A., Wynne, R., 2008. Free access to Landsat imagery. *Science* 320, 1011.
- Wu, H., Svoboda, M.D., Hayes, M.J., Wilhite, D.A., Wen, F., 2007. Appropriate application of the Standardized Precipitation Index in arid locations and dry seasons. *Int. J. Climatol.* 26, 65–79.
- Wulder, M.A., Hall, R.J., Coops, N.C., Franklin, S.E., 2004. High spatial resolution remotely sensed data for ecosystem characterization. *Bioscience* 54, 511–521.
- Wylie, B.K., Meyer, D.J., Tieszen, L.L., Mannel, S., 2002. Satellite mapping of surface biophysical parameters at the biome scale over the North American grasslands a case study. *Remote Sens. Environ.* 79, 266–278.
- Yang, F., White, M.a., Michaelis, A.R., Ichii, K., Hashimoto, H., Votava, P., Zhu, A.X., Nemani, R.R., 2006. Prediction of continental-scale evapotranspiration by combining MODIS and AmeriFlux data through support vector machine. *IEEE Trans. Geosci. Remote Sens.* 44, 3452–3461.
- Yao, J., Peters, D.P.C., Havstad, K.M., Gibbens, R.P., Herrick, J.E., 2006. Multi-scale factors and long-term responses of Chihuahuan Desert grasses to drought. *Landscape Ecol.* 21, 1217–1231.
- Zeileis, A., Grothendieck, G., 2005. zoo: S3 infrastructure for regular and irregular time series. *arXiv Prepr. math/0505527*.
- Zha, Y., Gao, J., Ni, S., Liu, Y., Jiang, J., Wei, Y., 2003. A spectral reflectance-based approach to quantification of grassland cover from Landsat TM imagery. *Remote Sens. Environ.* 87, 371–375.
- Zhu, Z., Woodcock, C.E., 2014. Automated cloud, cloud shadow, and snow detection in multitemporal Landsat data: an algorithm designed specifically for monitoring land cover change. *Remote Sens. Environ.* 152, 217–234.